frontiers | Frontiers in Environmental Science

ORIGINAL RESEARCH
published: 11 August 2022
doi: 10.3389/fenvs.2022.866152

The Effects of Engineered Aeration on Atmospheric Methane Flux From a Chesapeake Bay Tidal Tributary

Laura L. Lapham, Edward A. Hobbs, Jeremy M. Testa, Andrew Heyes, Melinda K. Forsyth, Casey Hodgkins, Curtis Szewczyk and Lora A. Harris*

Chesapeake Biological Laboratory, University of Maryland Center for Environmental Science, Solomons, MD, United States

Engineered aeration is one solution for increasing oxygen concentrations in highly eutrophic estuaries that undergo seasonal hypoxia. Although there are various designs for engineered aeration, all approaches involve either destratification of the water column or direct injection of oxygen or air through fine bubble diffusion. To date, the effect of either approach on estuarine methane dynamics remains unknown. Here we tested the hypotheses that 1) bubble aeration will strip the water of methane and enhance the air-water methane flux to the atmosphere and 2) the addition of oxygen to the water column will enhance aerobic methane oxidation in the water column and potentially offset the air-water methane flux. These hypotheses were tested in Rock Creek, Maryland, a shallow-water sub-estuary to the Chesapeake Bay, using controlled, ecosystem-scale deoxygenation experiments where the water column and sediments were sampled in mid-summer, when aerators were ON, and then 1, 3, 7, and 13 days after the aerators were turned OFF. Experiments were performed under two system designs, large bubble and fine bubble approaches, using the same observational approach that combined discrete water sampling, long term water samplers (OsmoSamplers) and sediment porewater profiles. Regardless of aeration status, methane concentrations reached as high as 1,500 nmol L^{-1} in the water column during the experiments and remained near 1,000 nmol L^{-1} through the summer and into the fall. Since these concentrations are above atmospheric equilibrium of 3 nmol L^{-1}, these data establish the sub-estuary as a source of methane to the atmosphere, with a maximum atmospheric flux as high as 1,500 µmol m^{-2} d^{-1}, which is comparable to fluxes estimated for other estuaries. Air-water methane fluxes were higher when the aerators were ON, over short time frames, supporting the hypothesis that aeration enhanced the atmospheric methane flux. The fine-bubble approach showed lower air-water methane fluxes compared to the larger bubble, destratification system. We found that the primary source of the methane was the sediments, however, *in situ* methane production or an upstream methane source could not be ruled out. Overall, our measurements of methane concentrations were consistently high in all times and locations, supporting consistent methane flux to the atmosphere.

Keywords: methane, aeration, eutrophication, estuary, OsmoSampler

OPEN ACCESS

Edited by:
Daniel F. McGinnis, Université de Genève, Switzerland

Reviewed by:
Peter Tango, United States Geological Survey (USGS), United States
Wei-Dong Zhai, Shandong University, China

****Correspondence:***
Laura L. Lapham
lapham@umces.edu

Specialty section:
This article was submitted to Biogeochemical Dynamics, a section of the journal Frontiers in Environmental Science

Received: *30 January 2022*
Accepted: *13 June 2022*
Published: *11 August 2022*

Citation:
Lapham LL, Hobbs EA, Testa JM, Heyes A, Forsyth MK, Hodgkins C, Szewczyk C and Harris LA (2022) The Effects of Engineered Aeration on Atmospheric Methane Flux From a Chesapeake Bay Tidal Tributary. Front. Environ. Sci. 10:866152. doi: 10.3389/fenvs.2022.866152

1 INTRODUCTION

The eutrophication of estuaries as a result of nutrient enrichment is a global phenomenon, with consequences that include deoxygenation and hypoxia (Diaz and Rosenberg, 2008). In fact, modeling and data analysis suggests that dissolved oxygen in estuaries will continue to decline into the future, primarily as a result of long-term warming (Breitburg et al., 2018; Ni et al., 2019; Whitney and Vlahos, 2021). The primary mitigation tool has been to enforce managed reductions of land-based nutrients in the United States (Linker et al., 2013) and in Europe (HELCOM, 2021), yet engineered solutions are also being considered (Conley et al., 2009; Lehtoranta et al., 2022). Engineered aeration efforts work by either destratifying the water column or directly injecting oxygen to the water (Harris et al., 2015; Stigebrandt et al., 2015; Koweek et al., 2020). This has also been commonly done in small lake systems (e.g., Martinez and Anderson, 2013; Hounshell et al., 2021) and reservoirs (McCord et al., 2016). While aeration should relieve the low oxygen problem to create habitat for metazoan life, prevent the noxious release of sulfide from sediments, and enhance coupled nitrification-denitrification, an additional potential consequence is that aeration could also enhance atmospheric methane emissions in estuaries. If this is true, methane emissions from estuaries that undergo aeration could be larger than currently considered in the global budget (Saunois et al., 2020). It is critical to constrain all sources of methane to the atmosphere since it is a powerful greenhouse gas (Forster et al., 2007; Dlugokencky, 2020). However, studies from an aerated freshwater reservoir show that the methane emissions were lower than a nearby natural reservoir (McClure et al., 2018; McClure et al., 2021). To date, this interplay between engineered aeration and methane fluxes in a natural estuary has not been rigorously tested.

Estuaries are dynamic environments, generating temporally and spatially-varying habitats in which methane producing and consuming processes occur. The primary source of methane is the underlying sediments, as in most organic rich environments (Martens and Berner, 1974; Reeburgh, 2007). However, there is an increasing appreciation for alternative sources such as demethylation of organic phosphonates (Karl et al., 2008), bacterial degradation of water column dissolved organic matter (Repeta et al., 2016) and/or production by phytoplankton (Bižić et al., 2020) that have not been fully explored in estuarine systems. In shallow-water, dynamic coastal and estuarine environments, methane can also be delivered with currents or tides from lateral sources (Bižić et al., 2020). While methane formed in the sediments can enter the water column through ebullition (Boudreau, 2012) or diffusion, nearly 85% of the methane produced within sediments is oxidized anaerobically before it reaches the sediment-water interface *via* microbially mediated reactions including sulfate reduction, nitrate reduction, and iron reduction (Froelich et al., 1979; Reeburgh, 2007). The remaining methane released from the sediments to the overlying water column can then be oxidized aerobically *via* methanotrophs (Hanson and Hanson, 1996). Thus a conceptual model for a healthy estuary shows a small methane flux to the atmosphere (**Figure 1A**). Alternatively, when estuarine waters are highly eutrophic, there is a breakdown in the aerobic biofilter in the water column and this results in an enhanced methane flux when the bottom waters go hypoxic and anoxic (Gelesh et al., 2016). Thus, under these conditions, there is a higher methane flux to the atmosphere (**Figure 1B**).

Under this simple conceptual model, it is enticing to speculate that if the bottom waters were re-oxygenated, this would return the aerobic biofilter to its normal state and lower the methane flux to the atmosphere. However, methane is a highly insoluble gas, and the mere addition of air bubbles (devoid of methane) and physical movement of the water during aeration could instead promote methane to dissolve into the rising bubbles and released to the atmosphere. In this case, the size of the air bubbles injected into the bottom waters could affect the magnitude of the atmospheric flux. For example, when the bubbles are large, the physical movement of the turbulent water would release large amounts of methane (**Figure 1C**). When the bubbles are small, there is the possibility for some of the oxygen to diffuse into the surrounding water (which is the goal of aeration systems) and promote aerobic methane oxidation (**Figure 1D**).

Oxygenated water columns are necessary for aerobic methane oxidizing bacteria to help control methane emissions to the atmosphere. In the simplest case of the open ocean where there are deep, well-oxygenated waters, nearly all the dissolved methane in the water column is oxidized (Leonte et al., 2017; Pohlman et al., 2017). Yet even in these systems, studies have shown there is a lag time for aerobic oxidation (Chan et al., 2019), with notable exceptions such as the rapid response of methanotrophs to methane released during events like the Deepwater Horizon oil spill (Kessler et al., 2011). Classic works have shown the highest rates of aerobic methane oxidation at the oxycline in arctic lakes (Rudd and Hamilton, 1978) suggesting that these organisms are facultative microaerophiles who work in these strong oxygen gradients (Oswald et al., 2015; Steinle et al., 2017). Aerobic methane oxidation can also proceed at high oxygen concentrations, especially when nitrogen is available. Under eutrophic conditions, when dissolved inorganic nitrogen concentrations >20 μM (M is used throughout as a symbol for mol L^{-1}), aerobic methane oxidation occurs at oxygen levels >31 μM; much higher than found in the oxyclines (Sansone and Martens, 1978). Along with nitrogen, micronutrients (especially copper) stimulate activity of methane oxidizing bacteria (Semrau et al., 2010). Not surprisingly the dissolved methane concentration in the environment has been shown to influence the rate of water column methane oxidation. For example, in Arctic waters, higher rates of methane oxidation were measured when higher concentrations of methane were available in summer (Mau et al., 2013). However, during the Deepwater Horizon oil spill, aerobic methane oxidation rates decreased over time after an initial spike, even though methane concentrations remained high (Crespo-Medina et al., 2014).

Here we present a study that quantified the effect of engineered aeration on air-water methane emissions from a eutrophic estuary. We leveraged a unique opportunity to manipulate whole ecosystem dissolved oxygen concentrations using two types of engineered destratification systems, that we

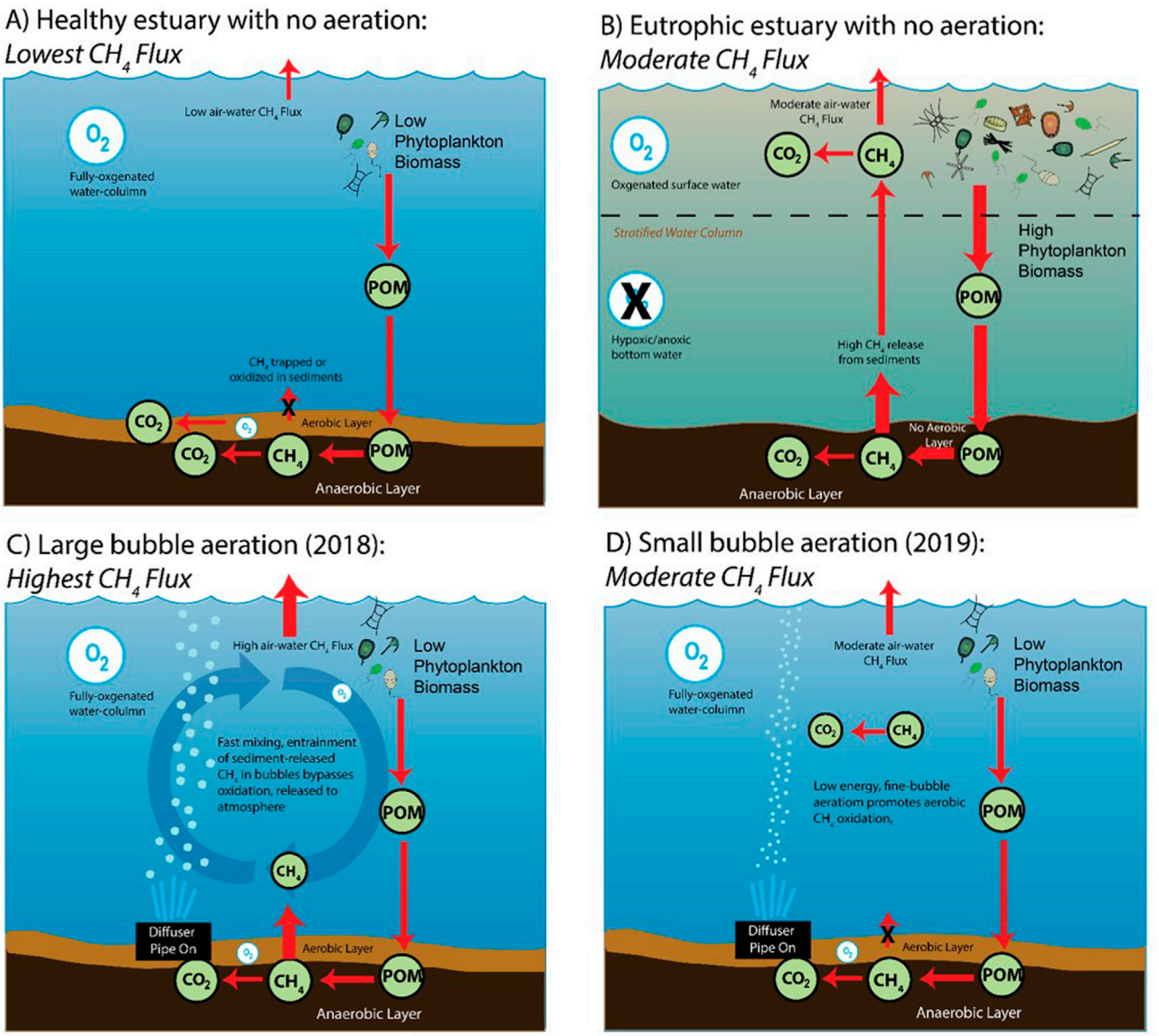

FIGURE 1 | Conceptual diagrams of methane dynamics in estuarine waters. With no aeration, **(A)** the lowest methane flux comes from a water column that is well oxygenated and **(B)** there is a moderate flux when waters are eutrophic. When aerated, the methane flux is **(C)** highest when there are large bubbles and **(D)** moderate when there are small bubbles.

distinguish based on the bubble size (large bubble and small bubble aeration). These systems provided an ideal opportunity to test the hypothesis that the physical disturbance introduced to a eutrophic system with bubbles will enhance the atmospheric methane flux (**Figures 1C,D**), regardless of oxygen concentration. We also surmised that the two different destratification systems would result in different methane fluxes to the atmosphere based on their bubble size; where the small bubbles would dissolve before reaching the air-water interface and not act as a transfer mechanism like larger bubbles. Furthermore, since the very idea behind engineered aeration is to add oxygen to the water column, we also hypothesized that aeration could enhance aerobic methane oxidation in the water column, which could act to lower the flux of methane to the atmosphere. To test our hypotheses, we conducted experimental manipulations of the aeration systems and sampled surface and bottom waters with aerators ON and then 1–13 days after the aerators were turned OFF. We hypothesized the source of methane in the water was the sediments, thus we also collected sediment cores at the same time. To put the discrete, experimental time points into a longer term context, we also present unique time-series measurements of methane concentrations in bottom waters across the whole estuary. Ultimately, this study contributes data to the growing literature of methane dynamics in shallow, eutrophic environments.

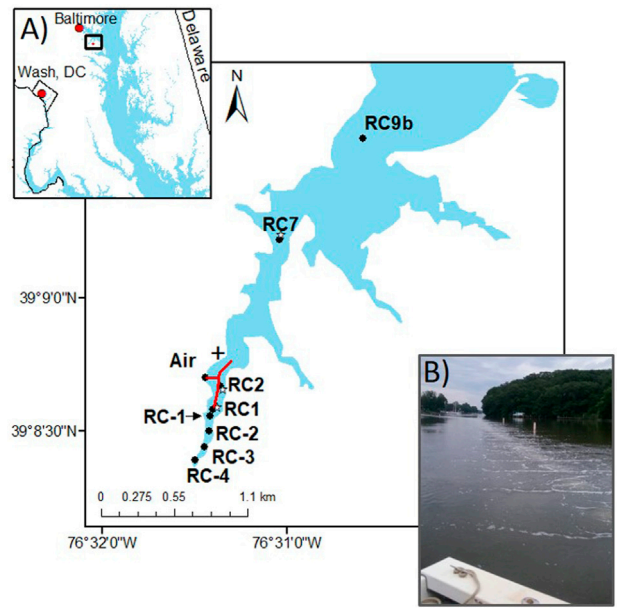

FIGURE 2 | Sample location map for Rock Creek. Red lines show location of the aeration tubes, black dots are water column and sediment station locations, white stars are OsmoSampler locations (very close to black dots), and black cross is location of dock where the benthic lander was deployed. **(A)** Location of Rock Creek (black square) in the northern Chesapeake Bay near Baltimore, Maryland. **(B)** Photo of bubbles breaking the surface in 2019 (photo by Laura Lapham).

2 MATERIALS AND METHODS

2.1 Field Description and Experimental Setup

The experiments were carried out in a 353-ha tidal tributary to the Chesapeake Bay found in Anne Arundel County, Maryland (**Figure 2**). Rock Creek's watershed is 80% residential and 20% forested. Due to the poor water quality over the past few decades (e.g., anoxia and extensive algal blooms), the county installed an engineered destratification system in 1988 to bring dissolved oxygen back to former levels (Harris et al., 2015). Herein, we call this the "large bubble aeration" system. Up until 2019, this system was made up of 138 ultra-coarse air diffusers distributed along a pipe that lines the middle creek channel with ~20 mm bubble size (CH2M_Hill, 2011), as described in design specifications reported by Dames and Moore (1988). The goal of the system was to vigorously overturn the water column in order to continuously introduce oxygen *via* de-stratification into the bottom waters, and the system was run continuously throughout the day. Every year, the aerators are turned on June 1 and turned off October 1, in order to minimize the effects of summertime hypoxia. An early study of this system determined that the zone of aeration influence was ~74 ha and that bottom waters remained oxic when diffusers were ON, but became anoxic within one tidal cycle when aerators were OFF (Harris et al., 2015; Harris et al., 2016). In spring 2019, the aeration system was upgraded to fine bubble diffusers to provide more oxygen to the water column, herein referred to as the "small bubble aeration" system. The goal of the diffusers is primarily to overturn the water to allow re-aeration to occur at the water surface, not to add oxygen from the bubbles themselves. There are two 213 m long diffusers emanating from the shore mainline, which provide air at a rate of 180 scfm (standard cubic feet per minute) in a continuous bubble pattern (0.26 scfm ft^{-1}) of bubbles 3 mm in diameter. The surface water expression of the new aeration system is shown in **Figure 2B**. With this new system, the county public works turns OFF the aerators every night to reduce neighborhood noise and energy consumption.

Over the course of 4 years (2016, 2018, 2019, 2021), the water column and sediments were sampled along the creek both within and outside the aeration zone and with both engineering designs (**Tables 1**, **2**). Stations within the aeration zone included RC1, which is located at the up-creek limit of aeration, and RC2 which is found mid-channel and directly in the aeration zone (**Figure 2**). RC7 is ~1 km downstream from the end of aeration, still within the zone of influence of aeration and where the creek widens, and RC9b is a background site, close to the mouth of the Patapsco River and outside the zone of influence of aeration (**Figure 2**). These stations were introduced in previous studies (Harris et al., 2015). Water depths are between 1.5–3.5 m. In 2021, four upstream stations were added to determine the river influence to the aeration zone (**Table 2**).

To study the effects of the aeration, our experimental approach was to sample while the aerators had been on for about 1 month, referred to as the "ON" sampling event, which occurred during the daylight hours. In the evening of the "ON" sampling, the aerators were turned off and waters sampled 1 day later (2016; large bubble aeration), 7 days later (2018; large bubble aeration), 13 days later (2019; small bubble aeration), and 3 days later (2021; small bubble aeration); these are referred to as the "OFF" sampling events (**Table 2**). After completion of the experiments, the aerators were turned back ON for the remainder of the season. By sampling at different time periods after aerators were turned OFF, the experiment addressed the question of the impact aeration had on methane flux from the Rock Creek estuary.

2.2 Sampling Description

During each field campaign, we collected water column hydrographic and chemical profiles, discrete water samples from the surface and bottom depths, and shallow (~30 cm) sediment cores *via* small boat. Water column temperature, salinity, and dissolved oxygen levels were recorded with a YSI

TABLE 1 | Station information.

Site	Latitude	Longitude	Water depth (m)
RC-4	39.13844	−76.52372	4
RC-3	39.13911	−76.52265	1.5
RC-2	39.14005	−76.52193	1.5
RC-1	39.14094	−76.52155	2.1
RC1	39.14133	−76.52122	2.1
RC2	39.14272	−76.52009	3.4
RC7	39.15108	−76.512	3.4
RC9b	39.15627	−76.50258	3.5

TABLE 2 | Overview of manipulation experiments.

Year	Date	Aeration status	Stations visited	System	CH_4[a] (nM)	DO[a] (mg L^{-1})	DIN[a] (μM)
2016	7/12/2016	ON	RC2,7	Large bubbles	324.1	4.0	21.2
	7/13/2016	OFF			351.1	2.3	20.3
2018	7/10/2018	ON	RC1,2,7,9b	Large bubbles	661.6	6.6	14.4
	7/11/2018	OFF			n.d	n.d	n.d
	7/11/2018	OFF			1,009.6	8.9	11.1
	7/17/2018	OFF			685.0	2.6	7.2
2019	7/9/2019	ON	RC1,2,7,9b	Small bubbles	337.2	6.6	27.8
	7/22/2019	OFF			834.1	6.2	4.9
2021	8/2/2021	ON	RC-4,-3,-2,-1,1,2,7,9b	Small bubbles	485.9	n.d	n.d
	8/6/2021	OFF			350.3	n.d	n.d

[a]*Methane, oxygen, and nitrogen values are averaged for stations RC1 and RC2 only. n.d. means not determined.*

EXO2 multiparameter sonde. In 2018, a benthic lander was placed at a dock (location shown as black cross in **Figure 2**) at the edge of the aeration zone that included continuous temperature, salinity, and dissolved oxygen sensors (YSI EXO2). Salinity is reported in practical salinity scale which has no units. Wind speeds were determined from a handheld anemometer (Weatherhawk, Windmate WM-200).

2.2.1. Discrete Water Column Samples

Water samples were collected for dissolved methane when the aerators were ON and OFF. Water samples were always taken within 1 m of the same GPS location. The sampling location is ~3 m off-axis to the aerators to ensure to not entangle the boat anchor. Therefore, when the aerators were ON, sampling never occurred in the bubble plume itself, always several meters away. Water column samples for dissolved methane concentrations were collected using published methods (Magen et al., 2014). Briefly, a submersible pump was placed at either 50 cm from the air-water interface, or 1 m from the sediment bottom and dispensed water into 125 mL glass serum vials by overfilling 5 times the vial volume and avoiding bubbles. The vials were then capped with thick butyl rubber septa and crimp sealed with aluminum rings. A 10 mL air (Ultra Zero Air purity, Airgas) headspace was given to the vials and then 0.5 mL 8 M KOH was added to arrest microbial activity during storage. The samples were stored upside down at 4°C until they could be measured back at the laboratory with a headspace equilibration technique. In 2021, water was collected with a slight modification to the method where the headspace equilibration step was conducted *in situ* and then the headspace physically separated from the water sample so no preservation was needed. Briefly, the submersible pump filled 120 mL into a 140 mL plastic syringe, bubble free. Then, 20 mL air (Ultra Zero Air purity, Airgas) was added and shook for 4 min to equilibrate. The temperature of the water was recorded for solubility calculations. Since this was a modification, we conducted efficiency tests using lab standards prior to the field campaign to verify 100% methane recovery from the method (**Supplementary Figure S1**). A complimentary water sample was also collected to quantify dissolved inorganic nitrogen (DIN) concentrations using published methods (Harris et al., 2015), in all years but 2021.

2.2.2. Sediments

Sediment cores were collected by hand off the side of the boat using a 6.5 cm diameter plexiglass cylinder attached to a pole. The cores were brought back to shore and immediately (within 1 h of sampling) sliced into 3 cm vertical sections and the sediment packed into 50 mL centrifuge tubes and stored at 4°C for later analysis of pore-water sulfate concentrations (Lapham et al., 2008b). A separate sample for dissolved methane in the pore-waters was also collected by subcoring each section with a 3 mL cut off plastic syringe and placing the material in a 13.5 mL glass serum vial, capped with butyl rubber septae and preserved with 3 mL 1 M KOH (Lapham et al., 2008b). Sediment samples were stored at −20°C until analysis.

2.2.3. Air Samples

At each station, a 140 mL plastic syringe was used to collect an air sample above the sampling site. In 2018, more air samples were collected over time because of opportunistic sampling. Notably, on the ON and OFF days, air samples were collected at all stations at dawn, during the day, and at dusk. Sampling in 2019 was synchronous with water and sediment sampling during the day only. The syringe was upwind of any boat traffic and flushed copiously to provide a clean sample, before any other sampling occurred and potentially contaminated the air. These air samples were stored at 23°C for less than 2 days before they were measured for methane concentrations and stable carbon isotope ratios.

2.2.4. Continuous Bottom Water Sampling

To capture the temporal variability of methane concentrations between sampling campaigns and after the aeration manipulation experiments were completed, bottom water was continuously collected using OsmoSamplers at RC1, RC2, and RC7. OsmoSamplers (**Supplementary Figures S2A,B**) are osmotically-driven pumps that continuously collect and store water in narrow bore copper capillary tubing (Jannasch et al., 2004). They have been used in numerous natural environments to quantify dissolved methane concentrations, including from deep water methane seeps (Lapham et al., 2008a; Wilson et al., 2015), estuaries (Gelesh et al., 2016), high altitude rivers (Buser-Young et al., 2021), high latitude wetlands (Buser-Young et al., 2022) and arctic lakes (McIntosh Marcek et al., 2021). Osmosis in the pumps

is created by an osmotic potential between a saturated brine chamber and freshwater chamber separated by semi-permeable membranes; no power is needed and there are no moving parts (Theeuwes and Yum, 1976; Jannasch et al., 2004). The osmotic pump is then connected to small-bore (0.082 cm inner diameter), long (up to 300 m) copper tubing coil, that is prefilled with freshwater. Water is then continuously drawn from the end of the copper tubing and stored in this tubing over time. The copper material is used so gases (i.e., methane) do not diffuse through it. The pumping rate is positively correlated to the surrounding water temperature and the number of membranes in the pump. For these deployments, two pump speeds were used. "Slow" pumps (8 membranes which pump 1 mL day^{-1}) were used for the long term collection of bottom water through the summer to give a temporal resolution of about 5 days (deployed for 9 months). "Fast" pumps (44 membranes which pump 5 mL day^{-1}) were used for a temporal high resolution of ~1 day (deployed for 1 week). For the slow pumps, we assume the sample stream undergoes plug flow; thus, dispersion within the tubing is minimal (Jannasch et al., 2004). For the fast pumps, plug flow may not be met, so we limited the deployment to a week. OsmoSamplers only collect water thereby precluding gas from affecting the sampler. The intakes are fitted with a 0.2 µm rhizone filter (Seeberg-Elverfeldt et al., 2005) to preclude microbes from the collection and alter the sample stream in the tubing during the deployment.

At the time of the deployment, the OsmoSamplers were attached to the copper coils and placed in a plastic crate (33 × 33 × 28 cm) under 16 kg weight and tied to a surface buoy (**Supplementary Figures S2C–E**). In 2018, the fast OsmoSampler sets were deployed at stations RC1, RC2, and RC7. In 2018, and 2019, slow OsmoSampler sets were also deployed at each of those stations along with Onset temperature and conductivity loggers. Because Rock Creek is a dynamic estuary, we used the conductivity detectors to verify the time-stamps in the OsmoSampler coils. OsmoSamplers were deployed from 9 July to 9 October 2018 and 18 June 2019 to 28 October 2019.

Upon recovery, the copper coils were sealed on either end with pliers and taken back to the lab to be stored at 4°C prior to further processing in the lab. The sensor data were downloaded. Within 1 week, the copper coils were unspooled and crimped into alternating lengths of 50 cm and 4.5 m using a wire crimping tool (Gelesh et al., 2016). The 50 cm sections were squeezed with a bench-top roller to flatten the copper tubing and force the liquid into 2 mL plastic tubes to immediately test for salinity using a handheld Extech RF20 refractometer. Because the coils were prefilled with freshwater before deployment, sectioning was terminated when zero salinity was observed for three samples in a row. These samples were also measured for chloride concentrations to compare to sensor conductivity measurements to verify time-stamps (Gelesh et al., 2016). The 4.5 m copper coil sections were squeezed using the bench-top hand roller which expressed sample liquid through a gastight adaptor and needle, and into a 13.5 mL glass sample vial at the opposite end, previously capped with a butyl rubber septum to prevent gas exchange, and flushed with helium. Each 4.5 m copper section contained approximately 2 mL of sample liquid that was transferred to the vials, resulting in an initial overpressure of approximately 2 mL. The dissolved CH_4 equilibrated with the helium headspace after shaking the vial for 2 min. Time stamps were calculated by adjusting pumping rates to *in situ* temperature, as shown in Gelesh et al. (2016). Unfortunately, the fast pumps only had 1 weeks' worth of tubing yet were deployed for 12 days due to weather delays. Thus, the pumps overpumped the coil and the first part of the deployment was lost.

2.3 Analytical Methods

For water column and sediment vial samples, the headspace was equilibrated with the dissolved methane from the aqueous sample and the headspace analyzed for the ppmv methane. For all samples, an aliquot of the headspace was extracted from the vials and injected onto a gas chromatograph (SRI 8610C multi-gas) equipped with a HayeSep D packed column and a Flame Ionization Detector in order to quantify methane concentrations (Magen et al., 2014). Certified standards (Airgas, Inc.) were used for the calibration curve. Analytical precision is 3% and all measurements were above detection limit of 2 ppmv. Resultant partial pressures were then used to calculate dissolved methane concentrations (in nM) in either the water column or the porewater using Henry's law according to equations in Magen et al. (2014) and porosity corrections according to Lapham et al. (2008a).

For sulfate and chloride concentrations in the sediment porewater samples, the tube containing whole sediment was centrifuged (3000 RPM, 30 min, 20°C, Sorvall© RT 6000D) and the resultant supernatant filtered with a 0.2 µm syringe filter. Samples were then diluted (1:135) in Milli-Q water and analyzed on a Dionex ICS 1000 ion chromatograph (IonPac AG22 4 × 50 mm guard column, IonPac AS22 4 × 250 mm analytical column, and ASRS 300 4 mm suppressor) with an AS40 Autosampler. Water samples from the 50 cm OsmoSampler sections were also measured for chloride with the same dilution to calculate salinity. Certified IAPSO seawater standard (Ocean Scientific International Ltd.) was used for the calibration curve. Analytical precision is 2% and all measurements were above detection limit of 0.05 mM for sulfate.

Air syringes were directly connected to the intake of a cavity ring down spectrometer (CRDS, Picarro 2201i) to measure for methane concentrations and methane stable carbon isotopes. For the water samples, 10 mL of degassed brine was added to the vials to displace the headspace and injected into the small sample isotope module (Picarro, Inc.) to introduce a small sample to the CRDS, similar to procedure in McIntosh Marcek et al. (2021). Isotope values were obtained through calibration with three Vienna Pee Dee Belemnite (VPDB) referenced standards (−23.9‰, −38.3‰, and −66.5‰ (±0.2‰); Isometric Instruments). Isotopic results are reported using the $\delta^{13}C$ notation in per mil (‰), where $\delta^{13}C = (R_{sample}/R_{standard} - 1) * 1{,}000$ and $R = {}^{13}C/{}^{12}C$. Analytical precision is 2% for concentrations and 4‰ for stable carbon isotope ratios.

2.4 Calculations

The air-water flux of CH_4, F, was determined for all discrete sampling campaigns using the updated flux equations presented Wanninkhof (2014):

$$F = k\left(C_w - C_{eq}\right) \quad (1)$$

where k is the gas transfer velocity (length time^{-1}), C_w is the measured surface water concentration, and C_{eq} is the CH_4 concentration in equilibrium with the atmosphere at *in situ* conditions (Yamamoto et al., 1976). There are several versions of **Eq. 1**, mostly based on wind speed. Here we employ the formulation and parameterization of Myllykangas et al. (2020), which reports a k value adapted from Raymond and Cole (2001):

$$k = 1.91\, e^{0.35u}\left(\frac{Sc}{600}\right)^{-0.5} \quad (2)$$

where u is the average wind speed and Sc is the Schmidt number for CH_4 in freshwater calculated from Wanninkhof (2014). Wind speeds were obtained from a nearby NOAA buoy (National Data Buoy Center BLTM2, Baltimore, MD) and averaged over the 3 days prior to sampling. Since the buoy is located 15 km away from Rock Creek, we compared the buoy to the handheld anemometer readings and found they compared within 7%. The buoy wind speed was used for all stations. Wind speeds varied between 2–3.2 m s^{-1}, which translated to k values varying between 3.8 and 5.9 cm h^{-1}, similar to values found in MacIntyre et al. (2010) in a lake system and mangrove dominated estuaries (Rosentreter et al., 2017). Air-water fluxes were then calculated using **Eq. 1** and reported as μmol CH_4 m^{-2} d^{-1}.

Since the calculated air-water flux is inherently based on assumptions of a stagnant boundary layer, the calculated air-water methane flux when the aerators are ON will be underestimated. To constrain this better when the aerators were ON, we calculated an air-water methane flux from direct bubble transport to surface water by applying the bubble radius of the system (3 mm, Mobley Engineering, Inc., personal communication) to an existing bubble model output to determine the mass transfer coefficient (**Figure 4** in McGinnis and Little, 2002). This mass transfer coefficient for the bubble radius in the system is 0.04 cm s^{-1} (or 144 cm h^{-1}) which was then used in **Eq. 1** to calculate a modified air-water methane flux for 2018 and 2019 at RC1 and RC2.

The sediment-water methane diffusive flux was calculated from Fick's first law:

$$J_{CH4-SWI} = -\varphi D_s \frac{dC}{dx} \quad (3)$$

where $J_{CH4\text{-}SWI}$ is the methane flux (μmol CH_4 cm^{-2} yr^{-1}) at the sediment-water interface, φ is the porosity (0.8), D_s is the sedimentary methane diffusion coefficient (cm^2 s^{-1}), x is the vertical sediment depth (cm) and dC/dx is the concentration gradient of methane. D_s was calculated for each station, corrected for tortuosity and *in situ* pressures (based on water depth), temperatures, and salinity (Millero, 1996), and was ~1.7 × 10^{-6} cm^2 s^{-1}. The gradient term was calculated between the uppermost porewater measurements; which usually started at 1.5 cm into the sediment. Thus, this gradient is most likely overestimated because it ignores any oxidation processes that might occur in that upper 1.5 cm of sediment. Using this gradient, the diffusive fluxes were then calculated for each station and time point with **Eq. 3**. For convenience, fluxes are reported as positive but represent flux out of sediment).

2.5 Box Model

We applied a simple box model to the flux data with the assumption that the sediments are the only source of methane to the water, and the atmospheric flux was the only sink of methane in the water. If the two balanced, then there would be no additional contributions to the methane budget in Rock Creek. If the fluxes did not balance, we could invoke additional microbial oxidation or production in the water column and/or advective transport of methane from up- or down-stream. To do this, at each station for 2018 and 2019, we subtracted the atmospheric methane flux from the sedimentary methane flux, then assigned the net difference as the water column methane inventory anomaly. For the aeration sites (RC1 and RC2), both air-water and sedimentary fluxes were averaged together. We should note that when the aerators are ON, we used the fluxes estimated from the stagnant boundary layer model which most likely underestimates the atmospheric flux.

2.6 Statistics

Student t-test was used in Excel (two-tailed, paired) to determine if the methane concentrations calculated from the discrete sampling events and the OsmoSampler samples were significantly similar. To create the paired methane dataset for this test, we extracted the OsmoSampler methane concentration that was sampled at the same time as the discrete methane measurement from the water column at each station. Please note that the OsmoSamplers average over 6–12 h. This comparison was done with the fast OsmoSamplers during 2018 (see **Section 3.6** for result).

3 RESULTS

3.1 Water Column Oxygen, Dissolved Inorganic Nitrogen, Temperature, and Salinity

The experimental design was intended to measure methane concentrations in well oxygenated, bubble-influenced waters when aerators were ON, and then hypoxic or anoxic waters without bubble transport when the aerators were turned OFF. Based on previous experiments in Rock Creek, the change to hypoxic conditions occurred within 1 day of turning off the aerators (Harris et al., 2015). However, for our manipulations, the goal was to observe changes over the longer term (up to 13 days) and the systems response. It is important to remember there was a 7-day difference between ON and OFF treatments in 2018 and 13-day difference in 2019.

In 2018 during aeration, the dissolved oxygen (DO) concentrations were ~7 mg L^{-1} at RC1 and RC2, and well mixed (**Figure 3** top panel). At RC7, the water column was still oxygenated (>4 mg L^{-1}; comparable to conditions at RC9b). After aerators were OFF for 7 days, RC1 and RC2 became hypoxic throughout the water column below 0.5 m, and the other stations had weakly stratified water columns, but with hypoxic bottom waters below 2.5 m.

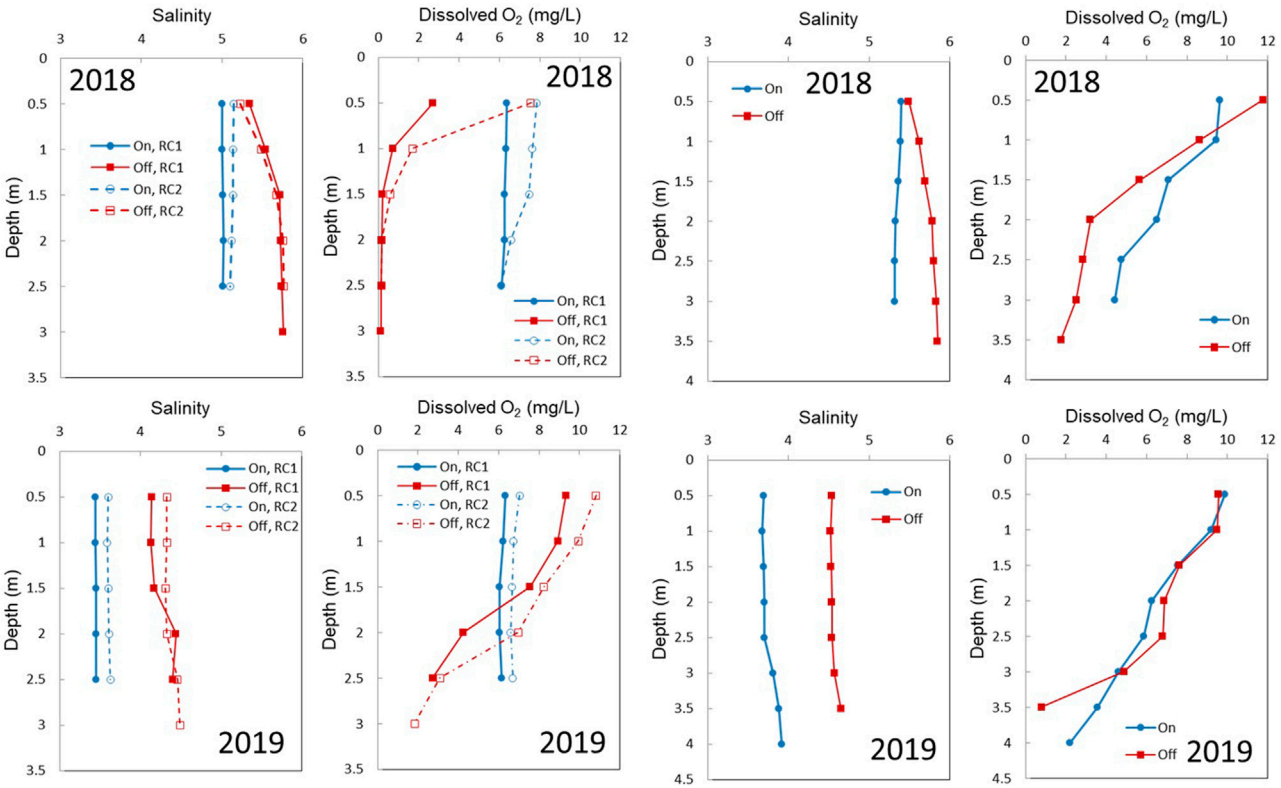

FIGURE 3 | Water column salinity and dissolved oxygen (O_2) profiles from 2018 (top panels) and 2019 (bottom panels) for stations within the aeration zone and stations outside the aeration zone. Blue symbols signify when aerators were ON and red when they were OFF.

Dissolved inorganic nitrogen concentrations averaged 14.4 μM (ranging between 0.8 and 19 μM for all stations) when aerators were ON and 7.2 μM (ranging between 3.7 and 12 μM) when aerators were OFF (**Table 2**). Salinity was ~5–5.5 (**Figure 3**). Water temperatures in 2018 varied between 26–30°C, and were similar for both ON and OFF treatments (data not shown).

In 2019, dissolved oxygen was relatively high in surface waters when the aerators were OFF at RC1 and RC2, giving way to oxygen-depleted conditions below 2 m (**Figure 3**). Dissolved inorganic nitrogen concentrations averaged 27.8 μM (ranging between 5 and 36 μM for all stations) when aerators were ON and 4.9 μM (ranging between 1 and 13 μM) when aerators were OFF (**Table 2**). Salinity was lower in 2019 than in 2018 and was nearly 3.5 when aerators were ON, and 4.5 when aerators were OFF (**Figure 3**). Water temperatures were between 26 and 29°C during the ON treatment and were warmer during OFF treatment (data not shown).

The tidal stage at each station varied over the discrete sampling time points (**Supplementary Figure S3**). In 2018 when aerators were ON, RC7 was sampled first at the ebbing tide, RC9b at low tide, and RC1 and RC2 at a high tide. When aerators were OFF, RC1 and RC2 were collected close to high tide or when waters were just beginning to ebb. RC7 and RC9b were sampled on the ebb tide. In 2019 when aerators were ON, RC9b, RC1, and RC2 were collected on flooding tide, and RC7 was collected right after high tide. When aerators were OFF, all stations were collected near the high tide.

3.2 Methane Concentrations and Stable Carbon Isotope Ratios in Water

Dissolved methane concentrations in surface and bottom water of Rock Creek varied over space and time (**Figure 4**). Overall, concentrations ranged between 150 and 1,500 nM, orders of magnitude higher than atmospheric equilibrium (which is ~3 nM), and were higher at stations RC1 and RC2, within the aeration zone, compared to stations closer to the Patapsco River (RC7, RC9b). In 2016, concentrations at RC2 and RC7 were around 400 nM throughout the period of measurements, regardless of aeration status (**Figure 4A**). In 2018, during aeration, the waters were relatively well mixed between surface and bottom waters (**Figure 4B**). Once aerators were turned OFF, there was an increase in bottom water methane at RC1 and RC2, and not much change at RC7 and RC9b. After 7 days, the surface waters were enriched in methane compared to the bottom water. In 2019, the concentrations between surface and bottom water followed expectations: during aeration, the water column was well mixed so there was little difference between surface and bottom waters and when aerators were turned OFF, methane

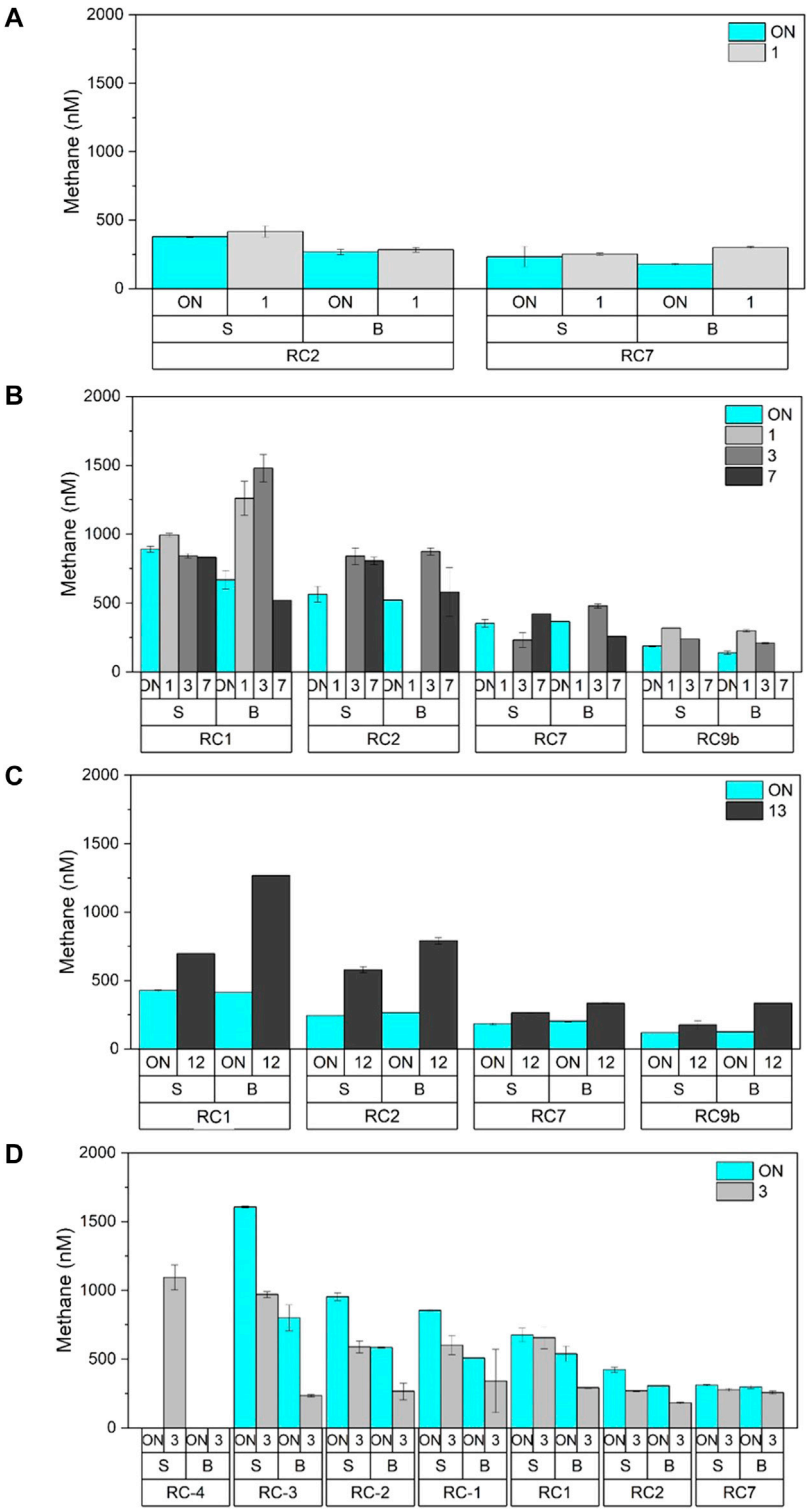

FIGURE 4 | Methane concentrations (colored bars) in surface (S) and bottom (B) water at all stations in **(A)** 2016, **(B)** 2018, **(C)** 2019, and **(D)** 2021. All blue colors represent the "ON" situation, and the gradients in gray color represent the number of days after aerators were turned off, which are described in each panel. Error bars represent standard error on replicate samples collected.

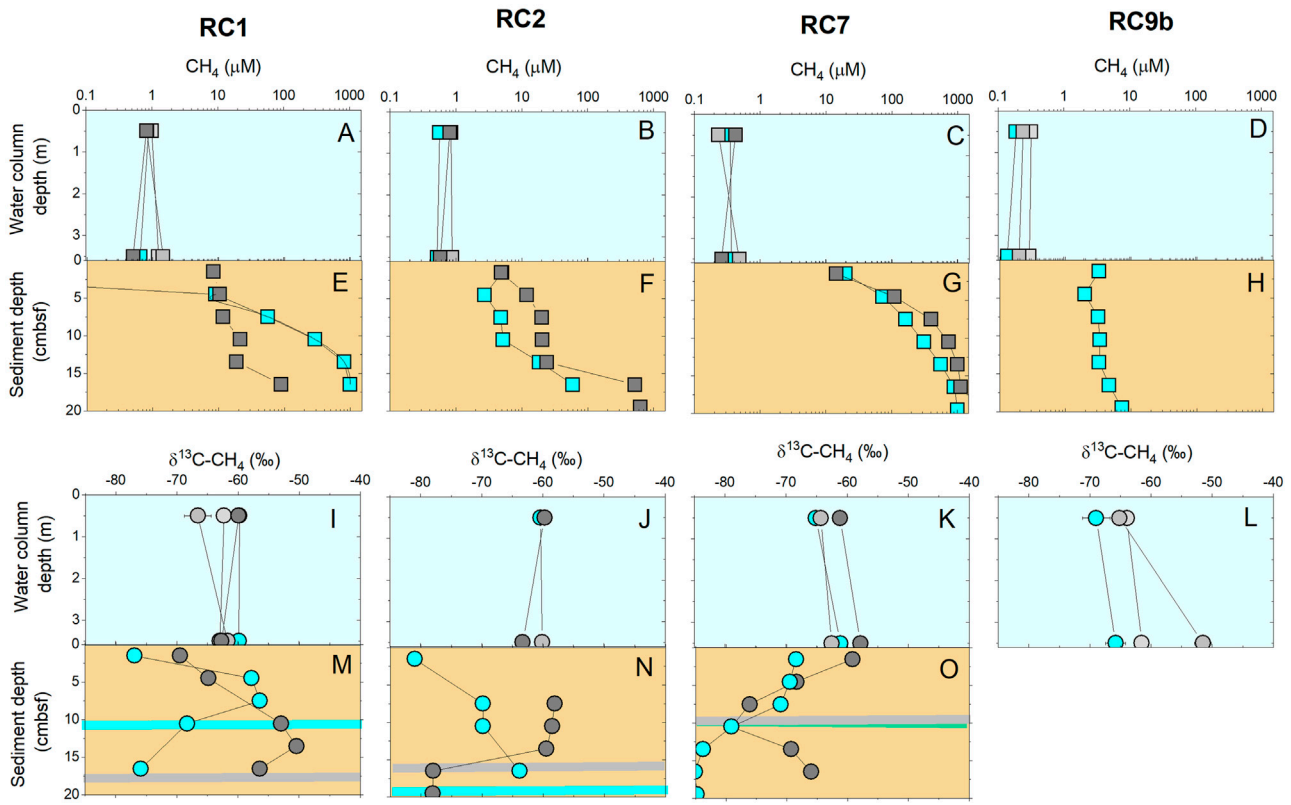

FIGURE 5 | In 2018, methane concentrations **(A–H)** and stable carbon isotopes **(I–O)** in water column (blue background) and in sediments (brown background). Blue symbol color denotes when aerators were on, and dark gray when they were off for 7 days. Horizontal bars in sediments **(M–O)** shows the movement of the sulfate-methane transition zone between ON (blue color) and OFF (gray color).

concentrations were higher in the bottom water than surface waters after 13 days (**Figure 4C**).

The 2021 field campaign was designed to resolve the upstream contribution of methane to the aeration zone. Overall, methane concentrations were lower than 2019 values but also showed the same pattern of higher concentrations at RC1 and RC2, than at RC7 (**Figure 4D**). At RC7, concentrations were similar between surface and bottom, and regardless of aeration status. At RC1 and RC2, methane concentrations were lower when aerators were OFF, which was unexpected. The other unexpected result was to record higher methane concentrations in surface waters than bottom waters during both ON and OFF periods (**Figure 4D**). Measurements made upstream of the aerators, which were only made in 2021, showed that surface waters were always higher than the bottom waters and that concentrations during the ON treatment were always higher than the OFF. Furthermore, methane concentrations were highest in the most upstream station, and declined downstream and into the estuary, such that water flowing into the aeration zone from upstream were enriched with methane relative to the aeration zone itself.

The water column methane concentrations are also presented in **Figures 5A–D**, **6A–D** as compilation figures showing the water column and sediments in a holistic view. Here we add to the water column concentration data the stable isotopic ratio of methane carbon to distinguish source of this methane (**Figures 5I–L**, **6I–L**). Regardless of station or aeration status, δ^{13}C-CH_4 values ranged from −69 to −51‰, with an average value of −61.4 ± 3.6‰, which is near the standard deviation of the method.

3.3 Sediment Porewater

Methane concentrations measured from the sediment porewaters increased with sediment depth (**Figures 5**, **6**, brown colored panels). Surface concentrations were at ~μM levels and increased to as high as 1,300 μM at the bottom of the core. In both years, concentrations were higher in the aeration zone (RC1 and RC2) and outside the aeration zone (RC7) compared to the background site (RC9b). Yet, there is variability in the sediment profiles. For example, at RC1 and RC2, sediment methane concentrations were lower in 2018 than in 2019, regardless of aeration status. After 13 days of no aeration, methane concentrations were higher in the sediments at RC2 and RC7. As noted, **Figures 5**, **6** also contain methane water column parameters for comparison purposes.

Methane increases in sediment porewaters are typically associated with a drawdown of sulfate in the surficial depths due to sulfate reducers outcompeting methanogens for substrates (Hoehler et al., 1994). Therefore, we also measured sulfate in porewater to help our understanding of anaerobic biogeochemical processing. Sulfate concentrations decreased downcore in all stations except RC9b although the depth of low sulfate (SO_4 < 0.5 mM) varied (**Supplementary**

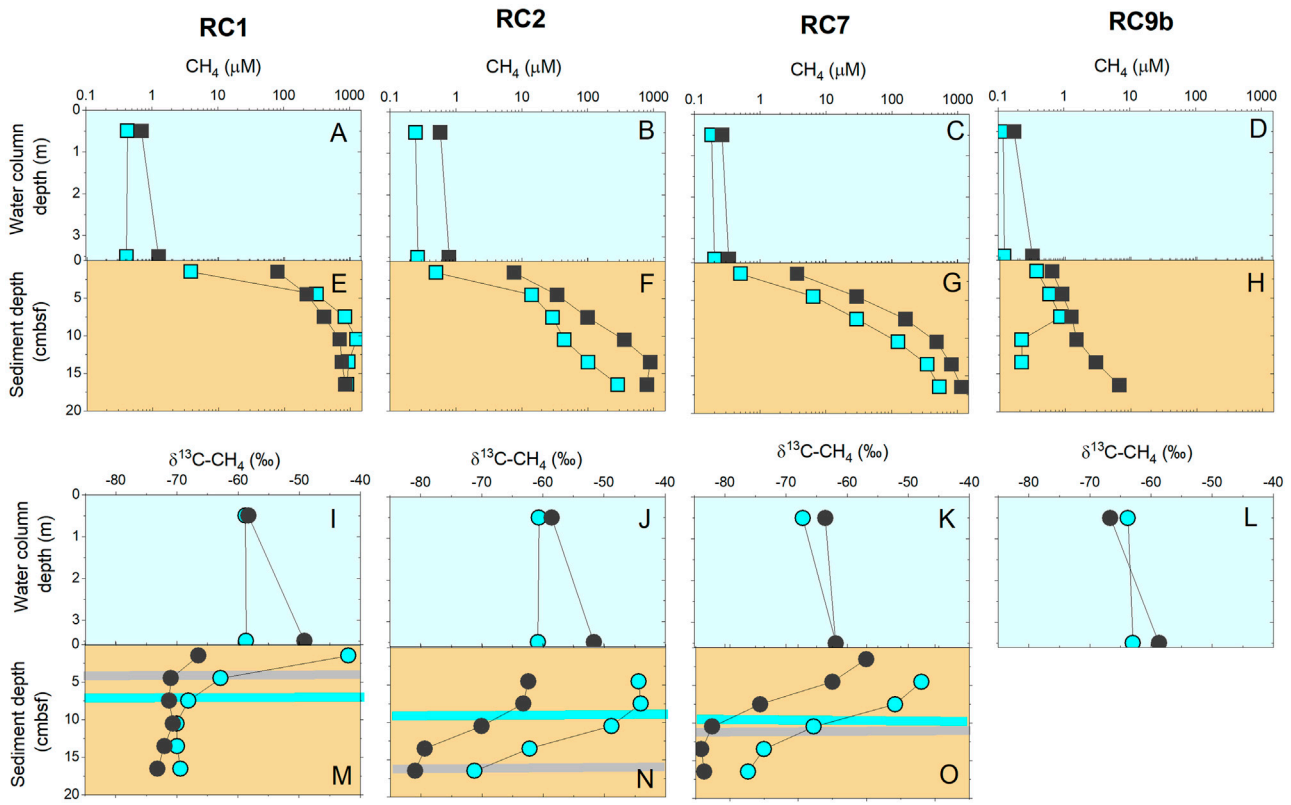

FIGURE 6 | In 2019, methane concentrations **(A–H)** and stable carbon isotopes **(I–O)** in water column (blue background) and in sediments (brown background). Blue symbol color denotes when aerators were on, and dark gray when they were off for 13 days. Horizontal bars in sediments **(M–O)** shows the movement of the sulfate-methane transition zone between ON (blue color) and OFF (gray color).

Figure S4). The depth of low sulfate typically coincides with the increase of methane, and is known as the sulfate methane transition (SMT) depth. The SMT is an area of active anaerobic methane oxidation *via* sulfate reduction (Jørgensen et al., 2020) and is a useful metric to show how active the anaerobic microbial community is in a sediment column (**Figures 5M–O**, **6M–O**). While we expected to see the SMT depth shoal when aeration was turned OFF, there was no consistent pattern of the depth of the SMT with aeration status for both years, although we will specifically present SMT depth patterns in each year below. Using the gradients from the top of the cores, the methane flux to the sediment-water interface varied across space and time, and ranged between 0.1 and 700 μmol m^{-2} d^{-1} (**Supplementary Figure S5**).

Chloride concentrations were also measured as a conservative tracer and as a way to validate any depletion of sulfate coming from sulfate reduction and not a consequence of groundwater. In 2018, while the chloride concentrations showed a slight increase in depth, the depth averages are as follows: 76 ± 8 mM (RC1, RC2), 100 ± 14 mM (RC7), and 85 ± 10 mM (RC9). Since these chloride values are within the range of what would be expected given the overlying water salinity, we represent any conservative mixing in terms of how it might affect sulfate concentrations. Given the rule of constant proportions, we calculated the range of sulfate values that would be estimated given those chloride concentrations (shaded rectangles in **Supplementary Figure S4**).

Methane stable carbon isotope ratios were measured to help distinguish the fate of methane formed in the sediment. Our measurements revealed two patterns in δ^{13}C-CH_4 values with depth: 1) δ^{13}C-CH_4 increasing with depth and 2) δ^{13}C-CH_4 peaks at intermediate depths associated with the SMT. In 2018, at RC1, the δ^{13}C-CH_4 values were similar during the ON and OFF conditions in that the surface was ^{13}C depleted (between −80 and −70‰), they became heavier with depth to as high as −50‰, and then decreased again to near surface sediment values (**Figure 5M**). The depth of the SMT deepened with aerators OFF. At RC2, during the ON condition, δ^{13}C-CH_4 values were ∼−80‰ and increased with depth in the core (**Figure 5N**). During the OFF condition, δ^{13}C-CH_4 values were around −60‰ in the shallow depths and quickly decreased to −80‰ at the SMT. At RC7, just outside the aeration zone, δ^{13}C-CH_4 values were ∼−70‰ at the surface when waters were aerated and decreased to −85‰ at the bottom of the core (**Figure 5O**). During the OFF situation, values showed a similar trend at the surface but then showed a mid-depth minimum of −80‰ at the SMT.

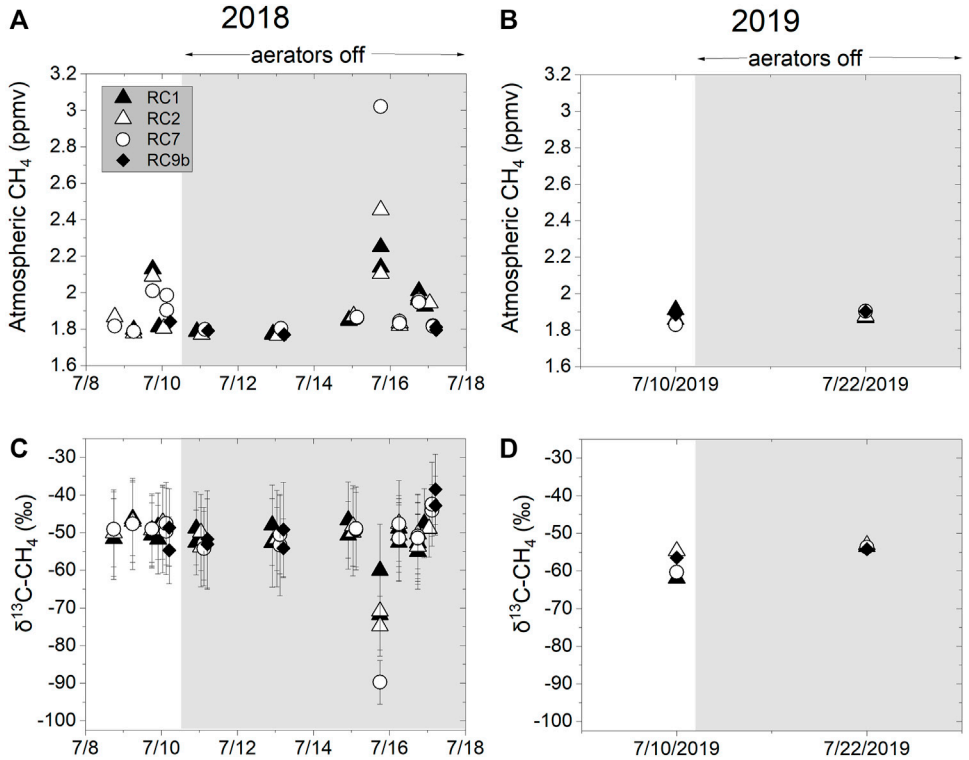

FIGURE 7 | Methane concentrations in air above the water in **(A)** 2018 and **(B)** 2019. δ^{13}C-CH_4 values in air above the water in **(C)** 2018 and **(D)** 2019. Shaded regions indicates when aerators were OFF.

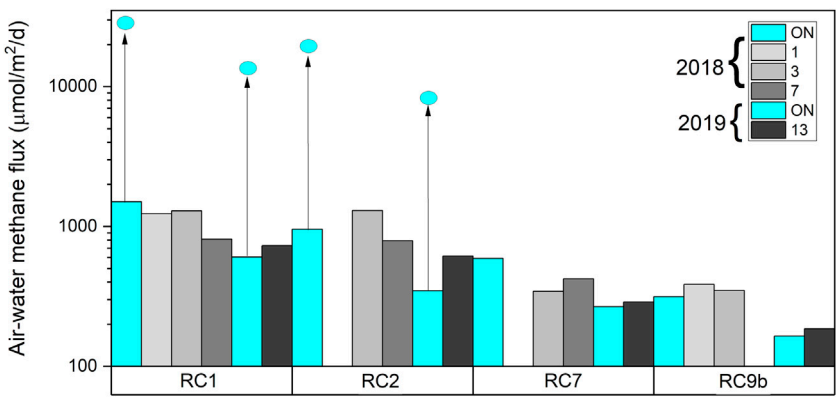

FIGURE 8 | Air-water methane flux for 2018 and 2019. Aerated waters are in blue, and non-aerated waters are shown in gray scale that corresponds to the number of days aerators were off. The bars indicate the flux calculated with the stagnant boundary layer model, whereas the extended arrows to the blue dots indicate the flux recalculated with bubble influence.

In 2019, the δ^{13}C-CH_4 value trends showed more consistency across the stations (**Figures 6M–O**). At RC1, values decreased at the surface from as high as −40 to ~ −70‰ where values remained for about 15 cm into the sediments (**Figure 6M**). RC2 and RC7 show almost the same isotope profiles where values decrease downcore, but the δ^{13}C-CH_4 values are ~10–15‰ higher when aerators were ON compared to when they were OFF (**Figures 6N,O**).

3.4 Methane Concentrations and Stable Carbon Isotope Ratios in Air and Air-Water Fluxes

Methane concentrations were measured in the air above each station during 2018 and 2019. In 2018, the average atmospheric methane concentration across all sites was 1.84 ± 0.06 ppmv, and

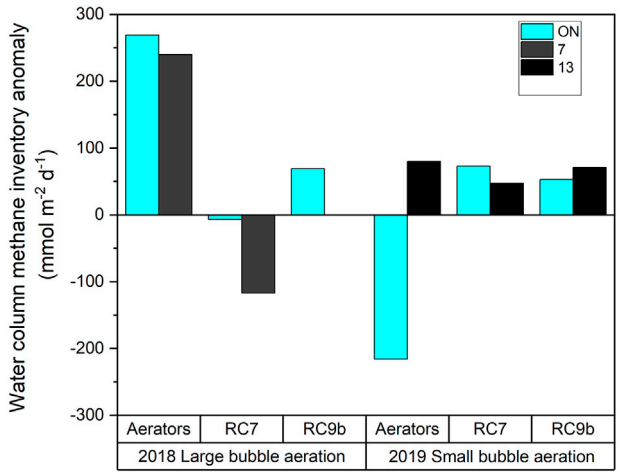

FIGURE 9 | Water column methane inventory anomaly assuming the sediments are the only source of methane to the water and the air-water interface is the only sink. A positive value means that there must be a source of methane to balance the source and sink, whereas the negative value means there must be a sink consuming methane.

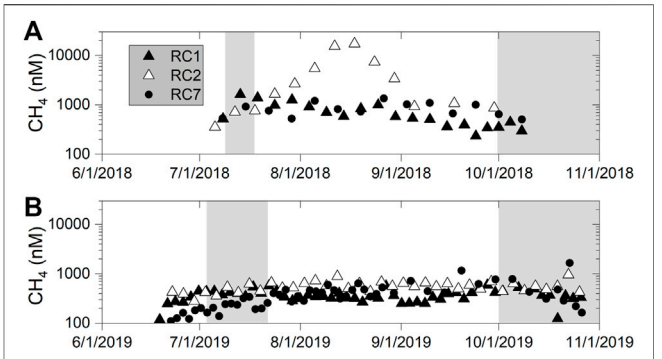

FIGURE 11 | Methane concentrations in bottom water in **(A)** 2018, and **(B)** 2019. Shaded region indicates when the aerators were turned off, otherwise, they were on.

didn't vary between ON and OFF conditions, except at the dawn sampling (**Figures 7A,B**). The average δ^{13}C-CH_4 value of the background methane was −51.4 ± 10‰ (**Figures 7C,D**). Dawn sampling on the ON and OFF days showed elevated methane concentrations, reaching as high as 3 ppmv at RC7 which had a δ^{13}C-CH_4 value of −90‰ (**Figures 7A,B**).

To calculate the air-water methane flux, we used two approaches. The first used the stagnant boundary layer model and most likely underestimates the flux for when the aerators are ON. Using this model, the air-water methane fluxes ranged between 300 and 1,500 μmol CH_4 m^{-2} d^{-1} (**Figure 8**). The flux was higher at RC1 and RC2 than other stations, regardless of aeration status or year. In 2018, the flux at the RC1 and RC2 was higher when aerators were ON after 7 days, whereas in 2019, the flux was lower when the aerators were ON. The second approach was only carried out when the aerators were ON and assumed methane was being stripped from the water as the aerator bubbles traveled up the water column. The calculated fluxes were much higher than the fluxes from the stagnant boundary layer (**Figure 8** extended arrows to blue dots). In 2018, at RC1 and RC2, air-water methane flux was 30,730 and 19,380 μmol CH_4 m^{-2} d^{-1}, respectively. In 2019, at RC1 and RC2, air-water methane flux was 14,669 and 8,342 μmol CH_4 m^{-2} d^{-1}, respectively.

3.5 Box Model Results

The sediment and air-water fluxes were used in the box model to determine if there are additional sources or sinks of methane beyond what is coming from the sediments and being lost to the atmosphere (**Figure 9**). In 2018, during large bubble aeration, there was a large source of methane (positive values in **Figure 9**) at the aerators, and actually a methane sink from RC7 when the aerators were off. In 2019, there was a methane source across all stations, regardless of aeration status, and this source was fairly

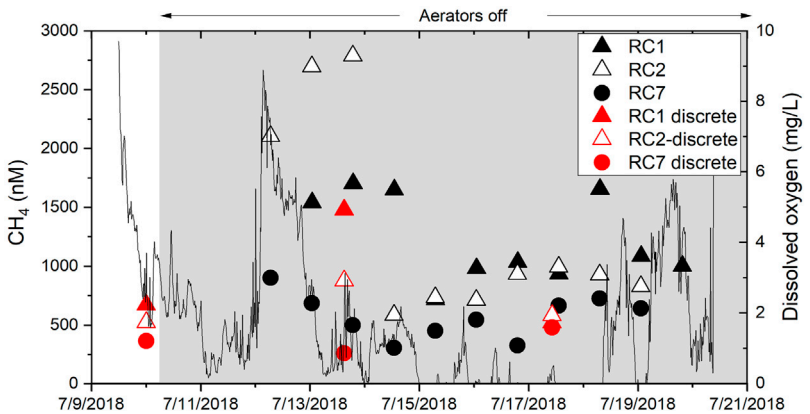

FIGURE 10 | Methane concentrations in high temporal resolution in bottom water from fast OsmoSamplers (black and white symbols) and discrete water samples (red symbols) in 2018 from stations RC1 (filled stars), RC2 (open stars), and RC7 (filled circles). Discrete samples overlap with OsmoSampler concentrations. Thin black line shows a dissolved oxygen record from sensors deployed in the bottom water off a nearby dock.

constant across the sites (**Figure 9**). The exception to this was at the aerators when they were ON; there was a large methane sink (negative value in **Figure 9**). However, since the atmospheric flux during the ON status is mostly likely underestimated, this exception is most likely a methane source too.

3.6 Time-Series Water Column Methane Measurements

Using OsmoSamplers, two separate records of dissolved methane concentrations from bottom water were obtained. The first was from the OsmoSampler deployment in 2018 that spanned 1-week using fast pumps with ~1 day resolution (**Figure 10**). The time stamps assigned were verified by comparing salinity (as calculated from chloride concentrations) in the OsmoSampler coils and the salinity from the sensor packages (**Supplementary Figure S6**). The salinity comparison shows relatively good agreement, especially at station RC7. The overall trend is similar between the sensor and OsmoSamplers at RC1 and RC2, but as we have observed in previous studies, the absolute salinity values did not match well at these stations (Gelesh et al., 2016). The highest methane concentrations came 3 days after the aerators were turned OFF at RC2 and reached almost 3,000 nM (**Figure 10**). Concentrations were also high at RC1 during this time. The timing of this methane peak came right after an event where dissolved oxygen (measured between stations RC2, and RC7) increased rapidly to ~8 mg L^{-1} oxygen (**Figure 10**). After 14 July 2018, methane concentrations decreased to less than 1,000 nM and were similar at all stations. Methane concentrations from OsmoSamplers were cross-checked with our discrete samples and we see no statistical difference between the two ($p = 0.72$); which is the first time this has been verified in field tests. Methane concentrations at RC7 remained lower than the other stations.

The second time-series record of methane concentration came from OsmoSamplers deployed through the summer and into the fall of 2018 and 2019, and contained slow pumps that give ~ weekly resolution (**Figure 11**). The temporal pattern was not the same each year. In 2018, at RC1 and RC2, the initial concentrations before aeration were lower (~400 nM), and then almost doubled when aerators were turned OFF (**Figure 11A**). Once they were turned back ON after our experiment, concentrations at RC1 continued to decrease at a rate of ~13 nM day^{-1} (linear fit with $R^2 = 0.8$); whereas at RC2, concentrations continued to increase through July and finally peak in August at 17,000 nM. Concentrations at RC2 then decreased and reached ~1,000 nM for the remainder of the timeseries. At RC7, concentrations didn't show much change with time and averaged 842 ± 265 nM. In 2019, we captured much higher temporal resolution with the samplers which started about 2 weeks before our experiment began (**Figure 11B**). Overall, concentrations were lower than in 2018 and ranged between 110 and 1,667 nM. There were concentration differences across sites, where methane concentrations at RC1 averaged 368 ± 100 nM; RC2 averaged 558 ± 136 nM; and RC7 averaged 400 ± 270 nM (**Figure 11B**). The bottom water temperature varied between 23–28°C in 2018 with some variability (**Supplmentary Figure S7**), whereas in 2019, the temperature gradually increased from ~23°C to a high of ~30°C in August and then decreased into the fall where a sudden decreased to less than 20°C occurred when the aerators were turned off (**Supplementary Figure S7**).

4 DISCUSSION

One solution to estuarine eutrophication is to artificially aerate the waters with bubble systems. This solution has benefits for reintroducing oxygen back into the water, but it could also have consequences for methane cycling. Previous studies have documented that the hypoxic or anoxic conditions in bottom waters that result from eutrophication also lead to the build-up of dissolved methane diffusing into the bottom waters from the sediments (Bange et al., 2010; Gelesh et al., 2016) which can result in a greater atmospheric flux. Thus, we hypothesized that when aerators are placed in such a system, the physical movement of all that water, with the fact that methane has low solubility, would enhance an atmospheric methane flux. To our knowledge, there is only one other study in a temperate lake that has studied oxygen effects on methane dynamics, and they found a remarkable decrease in methane build-up with engineered aeration (Hounshell et al., 2021), yet they did not quantify air-water flux. With our dataset, we were able to directly calculate this flux when the aerators were ON versus OFF to determine the impact of aeration in terms of methane dynamics. In addition to this, we also considered that the addition of oxygen to the water column might stimulate microbial aerobic methane oxidation which would somewhat control the release of methane at the air-water interface. Through our whole ecosystem manipulation experiment, we were able to address the following questions: 1) what is the effect of aeration on the atmospheric methane flux, 2) is Rock Creek an atmospheric methane source, 3) what is the source of water column methane in the Rock Creek, and 4) is aerobic methane oxidation enhanced in the water column? We also gained insights into complex biogeochemical processes and potential feedbacks occurring in this sub-estuary during and after aeration that sharpens our focus for future studies to further elucidate critical mechanisms related to dissolved oxygen dynamics and associated biogeochemical effects.

4.1 Aeration Enhanced Atmospheric Methane Flux

We hypothesized that the air-water methane flux would be higher during aeration then when the aerators were OFF. When we simply apply the stagnant boundary layer model to calculate the fluxes, we see that sites within the aeration zone (RC1 and RC2) had higher methane fluxes than downstream, regardless of aeration status (**Figure 8**). Yet these fluxes are most likely underestimates when the aerators are ON, as we see with the modified flux calculation (**Figure 8**, extended arrows to blue dots). We further hypothesized that under small bubble aeration, the flux would be lower than under large bubble aeration (**Figure 1**); which is what the fluxes showed in 2018 (large bubble aeration) versus 2019 (fine bubble aeration, **Figure 8**), supporting this hypothesis. The other observation was

TABLE 3 | Examples of estuarine flux of methane to the atmosphere.

Station	Air-water methane flux (mmol m^{-2} d^{-1})	References
Hudson River, NY Upper estuary	0.3	de Angelis and Scranton, (1993)
Hudson River, NY Lower estuary	0.6	de Angelis and Scranton, (1993)
Southern Baltic Sea	0.05–0.4	Bange et al. (1998)
European tidal estuaries	0.13	Middelburg et al. (2002)
Randers fjord, Denmark	0.04–0.4	Abril and Iversen (2002)
	0.002–4.9	Borges and Abril (2011)
Indian mangrove forest	0.01	Dutta et al. (2014)
Australian estuary	0.2	Maher et al. (2015)
Chesapeake Bay-June	0.2	Gelesh et al. (2016)
Chesapeake Bay-Sept	1.8	Gelesh et al. (2016)
Northwestern Borneo	0.001–7.6	Bange et al. (2019)
Chesapeake Bay, Rock Creek MD	0.2–1.5	This study

that in 2019, when the fine bubble aeration was installed, the air-water methane flux was lower during aeration then when the aerators were turned OFF. We have already stated that this flux is most likely underestimated. Future work would benefit from directly measuring this flux with floating chambers to more precisely quantify this flux.

4.2 Is Rock Creek an Atmospheric Methane Source?

Rock Creek is a source of atmospheric methane, regardless of aeration status, or site. The air-water methane flux from Rock Creek varied between 0.2 and 1.5 mmol m^{-2} d^{-1} (note change in units to compare to literature values), which was similar to fluxes measured from several estuaries (**Table 3**), and higher than those from oceanic environments, which vary between 0.0001 and 0.1 mmol m^{-2} d^{-1} (Bižić et al., 2020). Rock Creek methane fluxes are on par with a shallow subarctic lake which reached almost 0.4 mmol m^{-2} d^{-1} (Jansen et al., 2020), even though at times of ice-out, these lakes can release as much as 75 mmol m^{-2} d^{-1} (McIntosh Marcek et al., 2021). Surface water concentrations were also similar to those measured from an aerated eutrophic lake (Martinez and Anderson, 2013) suggesting methane is emitted in these aerated waters. A unique aspect to the work presented here is the high-frequency sampling over the warm season in Rock Creek which measured consistently high concentrations (400–1,000 nM) in the bottom water (**Figure 11**) that rival what has been measured in the anoxic bottom waters of the mainstem Chesapeake Bay in mid-summer (Gelesh et al., 2016) and further supports a sustained methane flux to the atmosphere. Thus this relatively shallow (~3 m) eutrophic estuary, may contribute more methane than previously thought, as was the case for streams and rivers (Stanley et al., 2016), and conforms to our understanding of coastal ecosystems as having an outsized influence on methane fluxes in a global context.

4.3 The Source of Methane: All From Sediments?

Sedimentary methanogenesis is likely the main source of methane to the water column of Rock Creek because the highest dissolved methane concentrations were measured in the sediments, and methane concentrations in the bottom water were typically higher than the surface water. Biogenic methane is also supported with the sedimentary porewater methane $\delta^{13}C\text{-}CH_4$ values in the deep sediments being < −70‰ (Whiticar, 1999). Yet, there was also evidence that methane produced in the deep sediments went through some degree of microbial oxidation before reaching the overlying water. The sediment porewater methane profiles showed classic concave-up shapes which are indicative of the anaerobic oxidation of methane (AOM) working in concert with sulfate reduction, as expressed here with the sulfate methane transition (SMT) depths (Jørgensen et al., 2019). AOM is also supported with the porewater methane isotopic composition data. In 2019, the porewater $\delta^{13}C\text{-}CH_4$ values also increased up the core through the SMT depth. This pattern indicates AOM; as the methane diffuses along the concentration gradient, microbial communities preferentially utilize ^{12}C and leave the ^{13}C behind (thereby values increase) as methane is oxidized (Whiticar, 1999). In 2019, this pattern is clear regardless of aeration status but there is a shift to more ^{13}C depleted values when aerators were OFF. This shift could represent enhanced microbial methane production when aerators were OFF but would need to be validated with other information such as diagenetic modeling (e.g., Martens et al., 1998). The 2019 sedimentary profiles, measured under the low-turbulence diffuse system, support our classic understanding of biogeochemical zonation (Froelich et al., 1979) and suggests that the sediments are diffusion dominated.

The pattern in 2018 was not as clear, possibly due to sediment disturbance with vigorous aeration. The destratification system employed during 2018 involved a high-volume through flow of air that leads to substantial physical disturbance of the water-column and sediments. Such disturbance at the aerators translated into variable porewater methane concentration and the isotope patterns, compared to outside the aeration zone (**Figure 5**). This implies that a simple, steady-state 1D, diffusion dominated interpretation of these profiles cannot be applied here because the destratification system could have driven substantial advective exchange between sediments and the water-column. It is interesting to note that at the aerators (RC1 and RC2), there was a depletion of ^{13}C up the core to the sediment-water interface. One way to inject such a depleted signature is by

methanogenesis which could happen in this agitated system by bubbling out deep methane during aeration or methanogenesis in the surface layers using non-competitive substrates (Alperin et al., 1988). More work would be needed to support or refute these possibilities.

Methane from the sediments can either diffuse into the overlying water or bubble out *via* ebullition (methane oversaturated porewaters forming bubbles). The methane released from both of those processes would have different isotopic signatures. For example, for bubbles to form in the sediments and efflux, the methane concentration must be above saturation which occurs in the sediments deeper than ~10 cmbsf, depending on the site and year (see **Figures 5**, **6**). At these depths, the $\delta^{13}C\text{-}CH_4$ values were between −80 and −85‰, so we would expect to see these values in the overlying water column (assuming a small amount of methane from the bubble equilibrates with the water). Bubbles captured in a shallow water column off North Carolina showed no isotopic fractionation when released to the water (Chanton and Martens, 1988). However, if the methane is diffusing into the water from the sediment surface, that methane would carry a $\delta^{13}C\text{-}CH_4$ value similar to the surface sediment methane signature. For 2018, the $\delta^{13}C\text{-}CH_4$ values of water column methane were always higher than the surface sediment, regardless of site or aeration status. This suggests that there could be some methane oxidation at the very sediment surface that we are missing in our sediment measurements. This was the same situation when the aerators were OFF in 2019. Perhaps future work could focus on the sediment-water interface as an area of intense methane oxidation, be it either aerobic or anaerobic.

The situation is a little different when the aerators were ON in 2019; the water column methane always had a lower $\delta^{13}C\text{-}CH_4$ value than the surficial sediments. This suggests that the methane was not simply diffusing in from the sediments, and that there must be another source of methane injecting isotopically depleted carbon; such as, sediment ebullition, methane being advected out of the sediments into the water column from the aerators, or microbial methane production in the water column. We don't have data to support or refute the advective release of methane out of the sediments other than to say that in 2019, the aeration was much finer and thus most likely less advective than in 2018 so it seems unlikely. Plus, since we were not focused on determining the ebullitive flux, its hard to evaluate. However, in 2018, we had evidence of an ebullitive flux of methane from the sediments. First, the methane in the air above Rock Creek waters had an average $\delta^{13}C\text{-}CH_4$ value of −50‰ which is slightly depleted in ^{13}C from the global, well-mixed value from the northern hemisphere of −47.4‰ (Lan et al., 2021). When this air $\delta^{13}C\text{-}CH_4$ value was compared to what was measured in the deep sediments, < −70‰, or in the water column, < −60‰, the ^{13}C depleted methane in air over Rock Creek waters can be explained with a small amount of biogenic methane from the sediments. Secondly, we measured a direct pulse of biogenic ($\delta^{13}C\text{-}CH_4$ = −80‰) methane in the air above RC7 at dawn when the aerators were OFF (**Figure 7**). This was most likely due to ebullition from the sediments directly reaching the atmosphere which was trapped in the air above the water due to the air inversion that occurs at dawn (Crill et al., 1988; Mukhophadhya et al., 2001). While this observation of high concentrations of methane in the morning air is not unexpected, it clearly documents how aqueous environments contribute to the atmospheric methane isotopic signal which has recently been shown to be enhanced in biogenic methane sources (Schaefer et al., 2016; Lan et al., 2021). It also clearly shows that in order to fully capture methane dynamics in this system, future work should quantify the bubble flux from the tributary, much like was done in the temperature lake in California (Martinez and Anderson, 2013).

4.4 Evidence for Methane Production in the Water Column

While we might have captured methane bubbling out of Rock Creek in 2018, that process is very heterogeneous and not continuous, and may not fully explain the water column $\delta^{13}C\text{-}CH_4$ values from 2019 ON status. We thus explore the possibility of water column methane production under aeration. There is growing evidence for an oxic production pathway in surface waters (see review in Bižić et al., 2020) that might be important. Most notably, it was concluded that 90% of methane in surface waters of a temperate lake was formed in the oxic surface waters, and not the sediments (Donis et al., 2017). However, a recent reevaluation of this work concluded that a sedimentary methane flux from the sediments flanking the lake in the shallow waters could explain the oversaturated surface waters (Peeters et al., 2019). In well stratified lakes, methane production in surface waters is shown to scale with sediment area and mixed layer volume (Günthel et al., 2019). Lakes are hydrodynamically very different from estuaries, making study comparisons to Rock Creek tenuous. Furthermore, the hydrodynamic conditions in destratification systems, such as in 2018, can create large cells of overturning water that may impact a much larger area of the tidal system (Gibbs and Howard-Williams, 2018). The lack of studies of sub-estuaries alone highlights the need to quantify the sources of methane from systems such as Rock Creek.

The box model, which balances sedimentary and air-water methane fluxes, shows that for most of the time, regardless of if aerators were ON or OFF, there is an additional methane source in the water column in 2019 (**Figure 11**). The observation that outside the aeration zone, RC7 and RC9, there is also an additional methane source could indicate the transport of methane from the Patapsco River, lateral inputs of water from across the creek as destratification cells pull in sources from a cross-section of the creek or simply upstream methane sources. Previous work in rivers also documented higher methane flux in upstream surface waters (de Angelis and Scranton, 1993; Abril and Iversen, 2002; Middelburg et al., 2002); as well as higher methane in smaller width creeks (Borges and Abril, 2011).

The further observation that there is a methane source regardless of the status of the aerators (either ON or OFF) suggests there is a bigger ecosystem response than just the influx of oxygen from the aerators. One possibility could be the presence of algal blooms which produce methane as a

byproduct (Bižić et al., 2020). Such blooms have been shown to occur before when aerators are turned OFF (Harris et al., 2015), and we also documented one right after the aerators were turned OFF in 2018 (**Figure 10**). Increased surface water oxygen levels were observed with an increase in particulate organic nitrogen and carbon, and iron (data not shown). The OsmoSamplers also captured a pulse of methane right after this oxygen pulse. If these blooms are a typical phenomenon right after turning the aerators OFF, it could explain why the methane fluxes were higher 3 days after turning aerators OFF in 2021 (**Figure 4D**) than when the aerators were ON. Future work could also directly quantify rates of methane production in aerobic waters.

4.5 Evidence for Aerobic Methane Oxidation in the Water Column?

While it seems clear that the aerators are enhancing a methane flux to the air above the creek, that the sediments are the main source of methane to the waters and there possibly is methane production in these aerated waters, we also considered if there is any microbially mediated oxidation in the surface waters that might offset this atmospheric flux. The idea here is that the waters are being oxygenated due to the aeration, as the oxygen data suggested happened during the experiment (**Figure 3**), and this oxygen is allowing for aerobic methane oxidation to happen. We have already speculated about a small potential oxidation process altering the $\delta^{13}C\text{-}CH_4$ from our surficial sedimentary methane values to the bottom water. Here, we focus solely on the water column. Since we didn't directly measure microbial rates, we need to rely on geochemical data. We did this in four ways. First, we interrogated the stable carbon isotopes of methane measured in the water column. The $\delta^{13}C\text{-}CH_4$ values give a bulk measure of what has happened to that methane since it was formed; the bulk methane signature would be more enriched in ^{13}C if it had been oxidized. In order to do this, we considered that the methane in the bottom water is the source for the methane in the surface water. **Figures 5**, **6** water column isotope profiles clearly show that in all cases, the surface water is always slightly ^{13}C depleted, if at all different, contrary to what would be found if aerobic methane oxidation was occurring. Secondly, we looked for a correlation between oxygen concentrations and methane concentrations. For this correlation, we surmised that if oxygen was controlling methane levels, we would see a linear relationship between the two. There was no correlation (**Supplementary Figure S8A**), which suggests oxygen is not the limiting factor for aerobic methane oxidation. Thirdly, we considered that maybe aerobic methane oxidation was limited by dissolved inorganic nitrogen (DIN), as has been proposed in the literature (Sansone and Martens, 1978). We surmise that if there is a negative relationship between DIN and water column methane concentrations, there could be evidence for aerobic methane oxidation. In other words, if methanotrophs were stimulated by DIN in an otherwise oxic water column, we would find low methane concentrations. This pattern did not emerge (**Supplementary Figure S8B**). And finally, in the box model approach described in **Section 4.3**, for most of the time in 2018 and 2019, there was a source of methane and not a sink. The exception was in 2019 when the aerators were ON. Taking all of this geochemical evidence into consideration, we conclude that we found little to no geochemical evidence for water column aerobic methane oxidation. Future work could focus on looking for microbial signature of oxidation in the water column.

4.6 Complicating Factors With Experimental Design

We have discussed the differences in atmospheric methane flux between the 2018 and 2019 aeration experiments to most likely be a factor of the bubble size during aeration. The large bubble aerators resulted in a larger flux of methane to the atmosphere than the small bubble aerators. However there were also differences between the 2 years in how long the aerators were turned OFF. Despite variability in the concentrations, we found almost no effect of aeration when the aerators were turned OFF for a few days (2016, 2021), but there was modest methane accumulation as oxygen was depleted for 3–7 days in 2018 and significant methane increases after 13 days in 2019. Thus, it appears that methane accumulation requires more than a day to emerge after deoxygenation, despite prior studies in Arctic lake systems (McIntosh Marcek et al., 2021) and in the Chesapeake Bay mainstem (Gelesh et al., 2016) that appear to indicate that methane is immediately released from sediments following deoxygenation. However, the temporal resolution of prior measures likely cannot capture day to day dynamics, and there are few, if any real-time measures of methane and oxygen in coastal systems to confirm the time-scale of methane responses to deoxygenation.

A second source of complication in our interpretations is that the experimental study is embedded in a system with background environmental variability. Thus, our "ON-OFF" study design using whole ecosystem manipulations does not offer a true controlled experimental system. For example, unlike previous work in Rock Creek (Harris et al., 2015), the waters did not go anoxic within 1 day in 2018 and 2019 and only at RC2 in 2018 did anoxia ever emerge. In 2018, there was also an influx of oxygen-rich water that appeared in the aeration zone within days after the aerators were turned OFF and when oxygen should have been depleted (seen in time series data on **Figure 10**). Although we did not measure methane during this event, the rapid increase in methane concentrations immediately after this pulse of tidally driven, oxygen-rich water could be the result of a rapid response to deoxygenation (that was not interrupted by the event) or an influx of methane rich water from upstream after the event. Our measurements in 2021 did indicate higher methane concentrations upstream of the aeration zone (~1,000 nM; **Figure 4D**), but these are substantially smaller than the concentrations measured after the event in 2018 (1,500 to 2,500 nM; **Figure 10**), suggesting that an upstream source is unlikely. Other potential inputs of methane are currently unknown, such as groundwater, and there are no substantial tidal wetlands that could serve as a methane source. Although

groundwater remains unlikely since chloride concentrations slightly increased with depth in sediment porewaters, our understanding of the drivers for the patterns remains elusive and long term observatories are needed.

Ecosystem responses to aeration beyond deoxygenation also likely feedback to influence methane dynamics in the estuary. Harris et al. (2015) reported a substantial algal bloom in Rock Creek within a week of the aerators being turned off, generating high surface water oxygen and organic matter concentrations. Given that Rock Creek has substantial light attenuation (Secchi Depth < 0.5), the vertical mixing induced by aerators likely keeps phytoplankton mixed below the photic layer, and when aerators are turned OFF, water-column stabilization allows for phytoplankton blooms. This is consistent with recent work in Chesapeake Bay that suggest that high chlorophyll-a packaging under low-light conditions combined with high nutrient concentrations allows for rapid algal growth when light becomes available (Buchanan, 2020). Methane concentrations reached the highest levels we measured at RC2 in 2018 (~2,700 nM), 3-days after an increase in particulate organic carbon of 700 μM after the aerators were turned OFF (data not shown). The consumption of this organic matter that likely followed may have generated substantial new methane, especially considering that oxygen concentrations were consistently below 32 μM (1 mg L^{-1}) for much of the following week (**Figure 10**). Given that the "destratification" approach used in 2018 was designed to physically mix and overturn the waters, such a phytoplankton response is likely. The "diffuse" approach used in 2019 involved much less physical disruption of the water-column (water-column salinity profiles were similar during ON and OFF), which may have prevented a phytoplankton response and also allowed for stable conditions that allowed the microbial communities to organize along expected redox conditions. This finding also points to an important impact of aerator design on our results, with differences in impact dependent on the mechanism of aeration and questions remain regarding how best to quantify mixing, oxygenation, and even water fluxes dependent on whether engineering impacted circulation (destratification design through large bubbles) versus diffusion of oxygen (small bubble aeration design).

5 CONCLUSION

There is evidence that the sediments are the main source of methane in Rock Creek as conceptualized in **Figure 1**, although we cannot rule out upstream creek waters or *in situ* production in the water column as additional sources. Our measurements suggest that aeration decreases the time frame available for aerobic methane oxidation in the water-column, thus connecting the sediment to the atmosphere more directly. This study did not allow for an in-depth examination of seasonal variations in methane sources and sinks, nor did it measure the impact of other complex factors on methane, such as shifting nutrient status and related microbial responses. Our experiments were also not intended to test aeration system design and operation (bubble size and density) in relation to methane flux, instead we used models to evaluate these impacts. Future work should 1) couple methane concentration and isotope data along with microbial rate measurements under various nutrient and oxygen conditions upstream and downstream of the aerators; 2) investigate seasonal changes to understand the complex factors controlling methane flux from this eutrophic estuary; and 3) characterize aerator design impacts on local hydrodynamics to better characterize physical effects on sediment transport and sediment-water exchange.

Keeping these recommendations in mind, the strength of our study can be distilled into two central findings we emphasize here: 1) The shallow, Rock Creek sub-estuary is a source of methane to the atmosphere, regardless of engineering intervention, and methane production and flux is likely enhanced as a consequence of eutrophication and 2) the strength of the methane flux is impacted by aeration bubble size design. Our conceptual model lays out the processes and impacts that are connected to these findings (**Figure 1**). The smallest fluxes occurred with the small bubble system (**Figure 9**), and we predict that continued implementation of this system combined with potential future oligotrophication could reduce methane fluxes. The largest fluxes occurred with the older, large bubble system that was intended to encourage destratification. The data support the hypothesis that aeration can lead to higher atmospheric methane fluxes and that aerator design is crucial to mitigating methane transfer. A key motivation for this study was to investigate the potential for unintended consequences of this engineering intervention in relation to greenhouse gas emissions. The dependency of the measured methane atmospheric fluxes on bubble size suggests that there is a path forward towards optimizing aerator design to reduce this consequence in eutrophic tidal waters (e.g., implement small bubble aeration). This study also adds to a growing body of literature quantifying methane fluxes in coastal waters. Regardless of aerator status or design, the current condition of Rock Creek as a eutrophic ecosystem characterized by high primary production of organic matter impacts its overall role as a source of methane to the atmosphere. As coastal water quality policies are implemented and managers seek both solutions and greater understanding of the complex biogeochemistry that impacts restoration trajectories in eutrophic systems, work on both engineering solutions and interpretation of restoration monitoring data would benefit from including methane dynamics and greenhouse gas impacts into holistic management frameworks.

DATA AVAILABILITY STATEMENT

The datasets presented in this study can be found in online repositories. The names of the repository/repositories and accession number(s) can be found below: https://www.ncei.noaa.gov/archive/accession/0244510.

AUTHOR CONTRIBUTIONS

LL, AH, JT, and LH conceived the idea; LL, CH, MF, CS, and EH conducted the experiment and analyzed samples; LL wrote the initial manuscript, and all authors contributed significant edits to the manuscript. We thank Mark Mobley for help with the bubble model, and the reviewers and editors who greatly improved this manuscript.

FUNDING

Financial support for this project was through U.S. National Science Foundation CBET-1706416 (LH, AH, JT, and LL), Maryland Sea Grant (NA14OAR4170090, SA75281450-O; LH and JT), and Maryland SeaGrant REU program (NSF grant OCE-1262374).

ACKNOWLEDGMENTS

We thank Anne Arundel county for access to the aerators, the residents of Rock Creek for allowing us to conduct the experiments in their backyard, and Janis Markusic for her support. The work could not have been done without the field help of Zachary Gotthardt, Lillian Henderson, and Brittany Clark and laboratory help of Maureen Strauss and Hadley McIntosh Marcek. We thank Dave Oliff at the Florida State University machine shop for building the fast OsmoSamplers. Work on this paper by Lapham was possible with the expertise and care of healthcare workers at the Johns Hopkins Breast Cancer Center and support from Marcia Lapham and Dr. Cédric Magen. Co-author Harris was supported by the Rock Creek team as a nursing mother in the field with patience, privacy, and good humor during boat work with co-authors Szewczyk and Testa. Lapham, Harris, and Testa depended on childcare provided by their communities and especially their spouses during the COVID-19 pandemic and are thankful to have had the time for this research. This is UMCES contribution #6188.

SUPPLEMENTARY MATERIAL

The Supplementary Material for this article can be found online at: https://www.frontiersin.org/articles/10.3389/fenvs.2022.866152/full#supplementary-material

REFERENCES

Abril, G., and Iversen, N. (2002). Methane Dynamics in a Shallow Non-tidal Estuary (Randers Fjord, Denmark). *Mar. Ecol. Prog. Ser.* 230, 171–181. doi:10.3354/meps230171

Alperin, M. J., Reeburgh, W. S., and Whiticar, M. J. (1988). Carbon and Hydrogen Isotope Fractionation Resulting from Anaerobic Methane Oxidation. *Glob. Biogeochem. Cycles* 2 (3), 279–288. doi:10.1029/gb002i003p00279

Bange, H. W., Dahlke, S., Ramesh, R., Meyer-Reil, L-A., Rapsomanikis, S., and Andreae, M. O. (1998). Seasonal Study of Methane and Nitrous Oxide in the Coastal Waters of the Southern Baltic Sea. *Estuar. Coast. Shelf Sci.* 47, 807–817.

Bange, H. W., Bergmann, K., Hansen, H. P., Kock, A., Koppe, R., Malien, F., et al. (2010). Dissolved Methane during Hypoxic Events at the Boknis Eck Time Series Station (Eckernförde Bay, SW Baltic Sea). *Biogeosciences* 7, 1279–1284. doi:10.5194/bg-7-1279-2010

Bange, H. W., Sim, C. H., Bastian, D., Kallert, J., Kock, A., Mujahid, A., et al. (2019). Nitrous Oxide (N2O) and Methane (CH4) in Rivers and Estuaries of Northwestern Borneo. *Biogeosciences* 16, 4321–4335.

Bižić, M., Grossart, H.-P., and Ionescu, D. (2020). "Methane Paradox," in *eLS* (Chichester: John Wiley & Sons).

Borges, A. V., and Abril, G. (2011). "Carbon Dioxide and Methane Dynamics in Estuaries," in *Treatise on Estuarine and Coastal Science*. Editors E. Wolanski and D. S. Mclusky (Waltham: Academic Press), 119–161. doi:10.1016/b978-0-12-374711-2.00504-0

Boudreau, B. P. (2012). The Physics of Bubbles in Surficial, Soft, Cohesive Sediments. *Mar. Petroleum Geol.* 38, 1–18. doi:10.1016/j.marpetgeo.2012.07.002

Breitburg, D., Levin, L. A., Oschlies, A., Grégoire, M., Chavez, F. P., Conley, D. J., et al. (2018). Declining Oxygen in the Global Ocean and Coastal Waters. *Science* 359 (46), 1–13. doi:10.1126/science.aam7240

Buchanan, C. (2020). A Water Quality Binning Method to Infer Phytoplankton Community Structure and Function. *Estuaries Coasts* 43 (4), 661–679. doi:10.1007/s12237-020-00714-3

Buser-Young, J. Z., Lapham, L., Thurber, A. R., Williams, K. H., and Colwell, F. S. (2021). Hidden Processes during Seasonal Isolation of a High-Altitude Watershed. *Front. Earth Sci.* 9 (6668199), 1–15. doi:10.3389/feart.2021.666819

Buser-Young, J. Z., Peck, E. K., Chace, P., Lapham, L. L., Vizza, C., and Colwell, F. S. (2022). Biogeochemical Dynamics of a Glaciated High-Latitude Wetland. *J. Geophys. Res. Biogeosci.* 127 (6), e2021JG006584. (accepted). doi:10.1029/2021JG006584

CH2M_Hill (2011). *Task4-Aeration Evaluation*. Annapolis: Maryland Department of Public Works.

Chan, E. W., Shiller, A. M., Joung, D. J., Arrington, E. C., Valentine, D. L., Redmond, M. C., et al. (2019). Investigations of Aerobic Methane Oxidation in Two Marine Seep Environments: Part 1—Chemical Kinetics. *J. Geophys. Res. Oceans* 124, 8852–8868. doi:10.1029/2019jc015594

Chanton, J. P., and Martens, C. S. (1988). Seasonal Variations in Ebullitive Flux and Carbon Isotopic Composition of Metahen in a Tidal Freshwater Estuary. *Glob. Biogeochem. Cycles* 2 (3), 289–298. doi:10.1029/gb002i003p00289

Conley, D. J., Bonsdorff, E., Carstensen, J., Destouni, G., Gustafsson, B. G., Hansson, L.-A., et al. (2009). Tackling Hypoxia in the Baltic Sea: Is Engineering a Solution? *Environ. Sci. Technol.* 43 (10), 3407–3411. doi:10.1021/es8027633

Crespo-Medina, M., Meile, C. D., Hunter, K. S., Diercks, A.-R., Asper, V. L., Orphan, V. J., et al. (2014). The Rise and Fall of Methanotrophy Following a Deepwater Oil-Well Blowout. *Nat. Geosci.* 7, 423–427. doi:10.1038/ngeo2156

Crill, P. M., Bartlett, K. B., Wilson, J. O., Sebacher, D. I., Harriss, R. C., Melack, J. M., et al. (1988). Tropospheric Methane from an Amazonian Floodplain Lake. *J. Geophys. Res.* 93 (D2), 1564–1570. doi:10.1029/jd093id02p01564

Dames and Moore (1988). The Rock Creek Estuary Study, Final Report. Prepared for the Anne Arundel County Watershed Management Program.

de Angelis, M. A., and Scranton, M. I. (1993). Fate of Methane in the Hudson River and Estuary. *Glob. Biogeochem. Cycles* 7 (3), 509–523. doi:10.1029/93gb01636

Diaz, R. J., and Rosenberg, R. (2008). Spreading Dead Zones and Consequences for Marine Ecosystems. *Science* 321 (5891), 926–929. doi:10.1126/science.1156401

Dlugokencky, E. (2020). *Global Methane Monthly Means*. [Online]. Available: https://www.esrl.noaa.gov/gmd/ccgg/trends_ch4/(Accessed January 1, 2021).

Donis, D., Flury, S., Stöckli, A., Spangenberg, J. E., Vachon, D., and McGinnis, D. F. (2017). Full-scale Evaluation of Methane Production under Oxic Conditions in a Mesotrophic Lake. *Nat. Commun.* 8 (1661), 1661–1712. doi:10.1038/s41467-017-01648-4

Dutta, M. K., Mukherjee, R., Jana, T. K., and Mukhopadhyay, S. K. (2014). Biogeochemical Dynamics of Exogenous Methane in an Estuary Assocaited to a Mangrove Biosphere; The Sundarbans, NE Coast of India. *Mar. Chem.* 170, 1–10.

Forster, P., Ramaswamy, V., Artaxo, P., Berntsen, T., Betts, R., Fahey, D. W., et al. (2007). *Changes in Atmospheric Constituents and in Radiative Forcing*. Cambridge, United Kingdom and New York, NY, USA: Cambridge University Press.

Froelich, P. N., Klinkhammer, G. P., Bender, M. L., Luedtke, N. A., Heath, G. R., Cullen, D., et al. (1979). Early Oxidation of Organic Matter in Pelagic Sediments

of the Eastern Equatorial Atlantic: Suboxic Diagenesis. *Geochim. Cosmochim. Acta* 43, 1075–1090. doi:10.1016/0016-7037(79)90095-4

Gelesh, L., Marshall, K., Boicourt, W., and Lapham, L. (2016). Methane Concentrations Increase in Bottom Waters during Summertime Anoxia in the Highly Eutrophic Estuary, Chesapeake Bay, U.S.A. *Limnol. Oceanogr.* 61 (S1), S253–S266. doi:10.1002/lno.10272

Gibbs, M. M., and Howard-Williams, C. (2018). "Physical Processes for In-Lake Restoration: Destratification and Mixing," in *Lake Restoration Handbook*. Editors D. P. Hamilton, K. J. Collier, J. M. Quinn, and C. Howard-Williams (Cham: Springer).

Günthel, M., Donis, D., Kirillin, G., Ionescu, D., Bizic, M., McGinnis, D. F., et al. (2019). Contribution of Oxic Methane Production to Surface Methane Emission in Lakes and its Global Importance. *Nat. Commun.* 10 (5497), 5497–5510. doi:10.1038/s41467-019-13320-0

Hanson, R. S., and Hanson, T. E. (1996). Methanotrophic Bacteria. *Microbiol. Rev.* 60 (2), 439–471. doi:10.1128/mr.60.2.439-471.1996

Harris, L. A., Hodgkins, C. L. S., Day, M. C., Austin, D., Testa, J. M., Boynton, W., et al. (2015). Optimizing Recovery of Eutrophic Estuaries: Impact of Destratification and Re-aeration on Nutrient and Dissolved Oxygen Dynamics. *Ecol. Eng.* 75, 470–483. doi:10.1016/j.ecoleng.2014.11.028

Harris, L. A., Day, M., and Hodgkins, C. (2016). *Rock Creek 2015 Water Quality Monitoring Results*. Technical report series No. TS-863-16. Solomons: University of Maryland Center for Environmental Science.

HELCOM (2021). *Baltic Sea Action Plan 2021 Update*. [Online]. Available: http://www.helcom.fi/(Accessed January 1, 2022).

Hoehler, T. M., Alperin, M. J., Albert, D. B., and Martens, C. S. (1994). Field and Laboratory Studies of Methane Oxidation in an Anoxic Marine Sediment: Evidence for a Methanogen-Sulfate Reducer Consortium. *Glob. Biogeochem. Cycles* 8 (4), 451–463. doi:10.1029/94gb01800

Hounshell, A. G., Mcclure, R. P., Lofton, M. E., and Carey, C. C. (2021). Whole-ecosystem Oxygenation Experiments Reveal Substantially Greater Hypolimnetic Methane Concentrations in Reservoirs during Anoxia. *Limnol. Oceanogr. Lett.* 6, 33–42. doi:10.1002/lol2.10173

Jannasch, H. W., Wheat, C. G., Plant, J. N., Kastner, M., and Stakes, D. S. (2004). Continuous Chemical Monitoring with Osmotically Pumped Water Samplers: OsmoSampler Design and Applications. *Limnol. Oceanogr. Methods* 2, 102–113. doi:10.4319/lom.2004.2.102

Jansen, J., Thornton, B. F., Cortés, A., Snöälv, J., Wik, M., MacIntyre, S., et al. (2020). Drivers of Diffusive CH4 Emissions from Shallow Subarctic Lakes on Daily to Multi-Year Timescales. *Biogeosciences* 17, 1911–1932. doi:10.5194/bg-17-1911-2020

Jørgensen, B. B., Beulig, F., Egger, M., Petro, C., Scholze, C., and Røy, H. (2019). Organoclastic Sulfate Reduction in the Sulfate-Methane Transition of Marine Sediments. *Geochim. Cosmochim. Acta* 254, 231–245. doi:10.1016/j.gca.2019.03.016

Jørgensen, B. B., Andren, T., and Marshall, I. P. G. (2020). Sub-seafloor Biogeochemical Processes and Microbial Life in the Baltic Sea. *Environ. Microbiol.* 22 (5), 1688–1706.

Karl, D. M., Beversdorf, L., Björkman, K. M., Church, M. J., Martinez, A., and Delong, E. F. (2008). Aerobic Production of Methane in the Sea. *Nat. Geosci.* 1, 473–478. doi:10.1038/ngeo234

Kessler, J. D., Valentine, D. L., Redmond, M. C., Du, M., Chan, E. W., Mendes, S. D., et al. (2011). A Persistent Oxygen Anomaly Reveals the Fate of Spilled Methane in the Deep Gulf of Mexico. *Science* 331 (6015), 312–315. doi:10.1126/science.1199697

Koweek, D. A., García-Sánchez, C., Brodrick, P. G., Gassett, P., and Caldeira, K. (2020). Evaluating Hypoxia Alleviation through Induced Downwelling. *Sci. Total Environ.* 719 (137334), 137334–137412. doi:10.1016/j.scitotenv.2020.137334

Lan, X., Nisbet, E. G., Dlugokencky, E. J., and Michel, S. E. (2021). What Do We Know about the Global Methane Budget? Results from Four Decades of Atmospheric CH4 Observations and the Way Forward. *Philos. Trans. R. Soc. Lond. Ser. A Phys. Sci. Eng.* 379 (20200440), 1–14. doi:10.1098/rsta.2020.0440

Lapham, L. L., Chanton, J. P., Martens, C. S., Higley, P. D., Jannasch, H. W., and Woolsey, J. R. (2008a). Measuring Temporal Variability in Pore-Fluid Chemistry to Assess Gas Hydrate Stability: Development of a Continuous Pore-Fluid Array. *Environ. Sci. Technol.* 42 (19), 7368–7373. doi:10.1021/es801195m

Lapham, L. L., Chanton, J. P., Martens, C. S., Sleeper, K., and Woolsey, J. R. (2008b). Microbial Activity in Surficial Sediments Overlying Acoustic Wipe-Out Zones at a Gulf of Mexico Cold Seep. *Geochem. Geophys. Geosyst.* 9 (6), Q06001. doi:10.1029/2008gc001944

Lapham, L. L., Strauss, M., Hobbs, E., Testa, J., Heyes, A., Forsyth, M., et al. (2021). *Methane (CH4) in Water, Methane (CH4) Stable Carbon Isotope Ratios, and Others in Rock Creek, Chesapeake Bay from 2016-07-12 to 2021-08-06 (NCEI Accession 0244510)*. Solomons: National Centers For Environmental Information. Available at: https://www.ncei.noaa.gov/archive/accession/0244510.

Lehtoranta, J., Bendtsen, J., Lännergren, C., Saarijärvi, E., Lindström, M., and Pitkänen, H. (2022). Different Responses to Artificial Ventilation in Two Stratified Coastal Basins. *Ecol. Eng.* 179 (106611), 1–13. doi:10.1016/j.ecoleng.2022.106611

Leonte, M., Kessler, J. D., Kellermann, M. Y., Arrington, E. C., Valentine, D. L., and Sylva, S. P. (2017). Rapid Rates of Aerobic Methane Oxidation at the Feather Edge of Gas Hydrate Stability in the Waters of Hudson Canyon, US Atlantic Margin. *Geochim. Cosmochim. Acta* 204, 375–387. doi:10.1016/j.gca.2017.01.009

Linker, L. C., Batiuk, R. A., Shenk, G. W., and Cerco, C. F. (2013). Development of the Chesapeake Bay Watershed Total Maximum Daily Load Allocation. *J. Am. Water Resour. Assoc.* 49 (5), 986–1006. doi:10.1111/jawr.12105

MacIntyre, S., Jonsson, A., Jansson, M., Aberg, J., Turney, D. E., and Miller, S. D. (2010). Buoyancy Flux, Turbulence, and the Gas Transfer Coefficient in a Stratified Lake. *Geophys. Res. Lett.* 37 (L24604), 1–5. doi:10.1029/2010gl044164

Magen, C., Lapham, L. L., Pohlman, J. W., Marshall, K., Bosman, S., Casso, M., et al. (2014). A Simple Headspace Equilibration Method for Measuring Dissolved Methane. *Limnol. Oceanogr.* 12, 637–650. doi:10.4319/lom.2014.12.637

Maher, D. T., Cowley, K., Santos, I. R., Macklin, P., and Eyre, B. D. (2015). Methane and Carbon Dioxide Dynamics in a Subtropical Estuary Over a Diel Cycle: Insights From Automated *in situ* Radioactive and Stable Isotope Measurements. *Mar. Chem.* 168, 69–79.

Martens, C. S., and Berner, R. A. (1974). Methane Production in the Interstitial Waters of Sulfate-Depleted Marine Sediments. *Science* 185 (4157), 1167–1169. doi:10.1126/science.185.4157.1167

Martens, C. S., Albert, D. B., and Alperin, M. J. (1998). Biogeochemical Processes Controlling Methane in Gassy Coastal Sediments-Part 1. A Model Coupling Organic Matter Flux to Gas Production, Oxidation and Transport. *Cont. Shelf Res.* 18, 1741–1770. doi:10.1016/s0278-4343(98)00056-9

Martinez, D., and Anderson, M. A. (2013). Methane Production and Ebullition in a Shallow, Artificially Aerated, Eutrophic Temperate Lake (Lake Elsinore, CA). *Sci. Total Environ.* 454-455, 457–465. doi:10.1016/j.scitotenv.2013.03.040

Mau, S., Blees, J., Helmke, E., Niemann, H., and Damm, E. (2013). Vertical Distribution of Methane Oxidation and Methanotrophic Response to Elevated Methane Concentrations in Stratified Waters of the Arctic Fjord Storfjorden (Svalbard, Norway). *Biogeosciences* 10, 6267–6278. doi:10.5194/bg-10-6267-2013

McClure, R. P., HamreHamre, K. D. A., Niederlehner, B. R., Munger, Z. W., Chen, S., Lofton, M. E., et al. (2018). Metalimnetic Oxygen Minima Alter the Vertical Profiles of Carbon Dioxide and Methane in a Managed Freshwater Reservoir. *Sci. Total Environ.* 636, 610–620. doi:10.1016/j.scitotenv.2018.04.255

McClure, R. P., Schreiber, M. E., Lofton, M. E., Chen, S., Krueger, K. M., and Carey, C. C. (2021). Ecosystem-Scale Oxygen Manipulations Alter Terminal Electron Acceptor Pathways in a Eutrophic Reservoir. *Ecosystems* 24, 1281–1298. doi:10.1007/s10021-020-00582-9

McCord, S. A., Beutel, M. W., Dent, S. R., and Schladow, S. G. (2016). Evaluation of Mercury Cycling and Hypolimnetic Oxygenation in Mercury-Impacted Seasonally Stratified Reservoirs in the Guadalupe River Watershed, California. *Water Resour. Res.* 52, 7726–7743. doi:10.1002/2016wr019061

McGinnis, D. F., and Little, J. C. (2002). Predicting Diffused-Bubble Oxygen Transfer Rate Using the Discrete-Bubble Model. *Water Res.* 36, 4627–4635. doi:10.1016/s0043-1354(02)00175-6

McIntosh Marcek, H. A., Lesack, L., Orcutt, B. N., Wheat, C. G., Dallimore, S., Geeves, K., et al. (2021). Continuous Dynamics of Dissolved Methane Over Two Years and its Carbon Isotopes (δ13C, Δ14C) in a Small Arctic Lake in the Mackenzie Delta. *J. Geophys. Res. Biogeosci.* 126 (3), 1–23. doi:10.1029/2020jg006038

Middelburg, J. J., Nieuwenhuize, J., Iversen, N., Høgh, N., de Wilde, H., Helder, W., et al. (2002). Methane Distribution in European Tidal Estuaries. *Biogeochemistry* 59, 95–119. doi:10.1023/a:1015515130419

Millero, F. (1996). *Chemical Oceanography*. Boca Raton, FL: CRC Books.

Mukhophadhya, S. K., Biswas, H., Das, K. L., De, T. K., and Jana, T. K. (2001). Diurnal Variation of Carbon Dioxide and Methane Exchange Above

Sundarbans Mangrove Forest, in NW Coast of India. *Indian J. Mar. Sci.* 30, 70–74.

Myllykangas, J.-P., Hietanen, S., and Jilbert, T. (2020). Legacy Effects of Eutrophication on Modern Methane Dynamics in a Boreal Estuary. *Estuaries Coasts* 43, 189–206. doi:10.1007/s12237-019-00677-0

Ni, W., Li, M., Ross, A. C., and Najjar, R. G. (2019). Large Projected Decline in Dissolved Oxygen in a Eutrophic Estuary Due to Climate Change. *J. Geophys. Res. Oceans* 124, 1–19. doi:10.1029/2019jc015274

Oswald, K., Milucka, J., Brand, A., Littmann, S., Wehrli, B., Kuypers, M. M. M., et al. (2015). Light-Dependent Aerobic Methane Oxidation Reduces Methane Emissions from Seasonally Stratified Lakes. *PLoS ONE* 10 (7), e0132574. doi:10.1371/journal.pone.0132574

Peeters, F., Encinas Fernandez, J., and Hofmann, H. (2019). Sediment Fluxes Rather than Oxic Methanogenesis Explain Diffusive CH4 Emissions from Lakes and Reservoirs. *Sci. Rep.* 9 (243), 243–310. doi:10.1038/s41598-018-36530-w

Pohlman, J. W., Greinert, J., Ruppel, C., Silyakova, A., Vielstädte, L., Casso, M., et al. (2017). Enhanced CO2 Uptake at a Shallow Arctic Ocean Seep Field Overwhelms the Positive Warming Potential of Emitted Methane. *Proc. Natl. Acad. Sci. U.S.A.* 114 (21), 5355–5360. doi:10.1073/pnas.1618926114

Raymond, P. A., and Cole, J. J. (2001). Gas Exchange in Rivers and Estuaries: Choosing a Gas Transfer Velocity. *Estuaries* 24 (2), 312–317. doi:10.2307/1352954

Reeburgh, W. S. (2007). Oceanic Methane Biogeochemistry. *Chem. Rev.* 107, 486–513. doi:10.1021/cr050362v

Repeta, D. J., Ferrón, S., Sosa, O. A., Johnson, C. G., Repeta, L. D., Acker, M., et al. (2016). Marine Methane Paradox Explained by Bacterial Degradation of Dissolved Organic Matter. *Nat. Geosci.* 9, 884–887. doi:10.1038/ngeo2837

Rosentreter, J. A., Maher, D. T., Ho, D. T., Call, M., Barr, J. G., and Eyre, B. D. (2017). Spatial and Temporal Variability of CO2 and CH4 Gas Transfer Velocities and Quantification of the CH4 Microbubble Flux in Mangrove Dominated Estuaries. *Limnol. Oceanogr.* 62, 561–578. doi:10.1002/lno.10444

Rudd, J. W. M., and Hamilton, R. D. (1978). Methane Cycling in a Eutrophic Shield Lake and its Effects on Whole Lake Metabolism. *Limnol. Oceanogr.* 23 (2), 337–348. doi:10.4319/lo.1978.23.2.0337

Sansone, F. J., and Martens, C. S. (1978). Methane Oxidation in Cape Lookout Bight, North Carolina. *Limnol. Oceanogr.* 23 (2), 349–355. doi:10.4319/lo.1978.23.2.0349

Saunois, M., Stavert, A. R., Poulter, B., Bousquet, P., Canadell, J. G., Jackson, R. B., et al. (2020). The Global Methane Budget 2000-2017. *Earth Syst. Sci. Data* 12, 1561–1623. doi:10.5194/essd-12-1561-2020

Schaefer, H., Fletcher, S. E. M., Veidt, C., Lassey, K. R., Brailsford, G. W., Bromley, T. M., et al. (2016). A 21-st Century Shift From Fossil-Fuel to Biogenic Methane Emissions Indicated by 13CH4. *Science* 352 (6281), 80–84. doi:10.1126/science.aad2705

Seeberg-Elverfeldt, J., Schlüter, M., Feseker, T., and Kölling, M. (2005). Rhizon Sampling of Porewaters Near the Sediment-Water Interface of Aquatic Systems. *Limnol. Oceanogr. Methods* 3, 361–371. doi:10.4319/lom.2005.3.361

Semrau, J. D., Dispirito, A. A., and Yoon, S. (2010). Methanotrophs and Copper. *FEMS Microbiol. Rev.* 34, 496–531. doi:10.1111/j.1574-6976.2010.00212.x

Stanley, E. H., Casson, N. J., Christel, S. T., Crawford, J. T., Loken, L. C., and Oliver, S. K. (2016). The Ecology of Methane in Streams and Rivers: Patterns, Controls, and Global Significance. *Ecol. Monogr.* 86 (2), 146–171. doi:10.1890/15-1027

Steinle, L., Maltby, J., Treude, T., Kock, A., Bange, H. W., Engbersen, N., et al. (2017). Effects of Low Oxygen Concentrations on Aerobic Methane Oxidation in Seasonally Hypoxic Coastal Waters. *Biogeosciences* 14, 1631–1645. doi:10.5194/bg-14-1631-2017

Stigebrandt, A., Liljebladh, B., de Brabandere, L., Forth, M., Granmo, Å., Hall, P., et al. (2015). An Experiment with Forced Oxygenation of the Deepwater of the Anoxic By Fjord, Western Sweden. *Ambio* 44 (1), 42–54. doi:10.1007/s13280-014-0524-9

Theeuwes, F., and Yum, S. I. (1976). Principles of the Design and Operation of Generic Osmotic Pumps for the Delivery of Semisolid or Liquid Drug Formulations. *Ann. Biomed. Eng.* 4 (4), 343–353. doi:10.1007/bf02584524

Wanninkhof, R. (2014). Relationship between Wind Speed and Gas Exchange Over the Ocean Revisited. *Limnol. Oceanogr. Methods* 12, 351–362. doi:10.4319/lom.2014.12.351

Whiticar, M. J. (1999). Carbon and Hydrogen Isotope Systematics of Bacterial Formation and Oxidation of Methane. *Chem. Geol.* 161, 291–314. doi:10.1016/s0009-2541(99)00092-3

Whitney, M. M., and Vlahos, P. (2021). Reducing Hypoxia in an Urban Estuary Despite Climate Warming. *Environ. Sci. Technol.* 55, 941–951. doi:10.1021/acs.est.0c03964

Wilson, R. M., Lapham, L. L., Riedel, M., Holmes, M. E., and Chanton, J. P. (2015). Observing Methane Hydrate Dissolution Rates Under Sediment Cover. *Mar. Chem.* 172, 12–22. doi:10.1016/j.marchem.2015.03.004

Yamamoto, S., Alcauskas, J. B., and Crozier, T. E. (1976). Solubility of Methane in Distilled Water and Seawater. *J. Chem. Eng. Data* 21 (1), 78–80. doi:10.1021/je60068a029

Conflict of Interest: The authors declare that the research was conducted in the absence of any commercial or financial relationships that could be construed as a potential conflict of interest.

Publisher's Note: All claims expressed in this article are solely those of the authors and do not necessarily represent those of their affiliated organizations, or those of the publisher, the editors and the reviewers. Any product that may be evaluated in this article, or claim that may be made by its manufacturer, is not guaranteed or endorsed by the publisher.